ORIGINAL RESEARCH

Poly(3-hydroxi-butyrate-co-3-hydroxy-valerate) (PHB-HV) microparticles loaded with holmium acetylacetonate as potential contrast agents for magnetic resonance images

Mariangela de Burgos M de Azevedo[1]
Vitor HS Melo[1]
Carlos RJ Soares[1]
Lionel F Gamarra[2]
Caio HN Barros[3,4]
Ljubica Tasic[4]

[1]Centro de Biotecnologia, IPEN/CNEN-SP, São Paulo, Brazil; [2]Hospital Israelita Albert Einstein, São Paulo, SP, Brazil; [3]School of Chemical and Bioprocess Engineering, University College Dublin, Dublin, Ireland; [4]Instituto de Química, UNICAMP, SP, Campinas, Brazil

Introduction: Biodegradable polymers that contain radioactive isotopes such as Holmium 166 have potential applications as beta particle emitters in tumor tissues. Also, Ho(III) is paramagnetic, which makes it suitable as a contrast agent for magnetic resonance (MR) images.

Methods: Holmium acetylacetonate ($Ho(acac)_3$) loaded poly(3-hydroxy-butyrate-co-3-hydroxy-valerate) microspheres, with 5% or 8% of 3-hydroxy-valerate (HV), were prepared by emulsification/evaporation process within 20–53 μm size. Microspheres characterization was done using scanning electron microscopy, energy-dispersive X-ray, and infrared spectroscopies. The release of holmium(III) in sodium phosphate buffer (pH 7.4) was followed for 9 days with inductively coupled plasma. Finally, T_2 and T_2* magnetic resonance images (MRI) were acquired and compared with the MRI of the inclusion complex of holmium acetylacetonate in some β-cyclodextrins.

Results: Holmium acetylacetonate loading, evaluated by thermogravimetry, was up to 20 times higher for copolymer with 5% of HV. It was shown that microspheres loaded with $Ho(acac)_3$ exhibited an accumulation of Ho(III) on their surfaces but were stable over time, as no expressive release of holmium(III) was detected in 9-day exposition to sodium phosphate buffer. Holmium acetylacetonate in both microspheres or inclusion complexes was very efficient in obtaining T_2 and T_2* weighted images in magnetic resonance, thus, might be used as contrast agents.

Conclusion: This is the first description of the use of inclusion complexes of holmium acetylacetonate in biodegradable polymers as contrast agents. New investigations are underway to evaluate the resistance of PHB-HV polymer microparticles to nuclear activation to assess their potential for use as radiopharmaceuticals for the treatment of liver cancer.

Keywords: holmium acetylacetonate, PHB-HV microparticles, microspheres, MRI

Introduction

The concept of nano- or microtechnological materials involves ones with sizes in the range of 1–100 nm or up to tenths of millimeters, respectively, and their application in human health is growing rapidly.[1] Cancer is a critical public health problem worldwide that has brought great burden to society. In 2016, around 1,685,210 new cases and 595,690 cancer deaths occurred just in the United States.[2] Many of the known cancer therapy modalities, such as chemo-, radio-, photodynamic therapy among others, apply substances or materials that can be classified in one of the above cited categories.[3,4] A great number of substances able

Correspondence: Mariangela de Burgos M de Azevedo
Centro de Biotecnologia, IPEN/Cnen-SP, São Paulo, Brazil, 05508-000
Email mariangela.burgos@cnpq.pq.br

to inhibit key enzymes, cytoskeleton synthesis, or with antimitotic, apoptotic and necrotic activities are used in cancer treatments, such as etoposide, teniposide, taxol, methotrexate, cisplatin, and derivatives.[5–10] All of these compounds belong to nano- or micro-world. Tumors' treatments and choices of specific therapeutic modality depend on tumor sensitivity. For example, to minimize maleficent effects in radiotherapeutic techniques, radionuclides, and radioisotopes can be complexed into microtechnological materials made from pure mixtures or composites.

Radioactive decays are hardly supported by cancer tissues. By stopping an essential metabolic process or inducing apoptosis, tumor tissues are quickly destroyed by direct or indirect effects of radioactive particles, gamma rays, auger electrons release, and generation of free radicals.[11] Alpha and beta particles, as well as gamma rays, propagate in a great range, and thus have more potential to destroy cancer tissues. One of the most suitable targets to beta particles is the water molecule and hydroxyl radical is the first of many new high-energy species and other radicals that destroy cell structures.[12] The high-energy alpha particles propagate less in tissues but cause more irreparable damages in the genetic material, while high-energy gamma radiation breaks chemical bonds.[13]

However, all kind of therapeutic agents usually explored to eliminate cancer are also absorbed by healthy cells: patients may suffer side effects as physical weakening, necrosis or burns depending on the method used. Thus, micro- and nanotechnology concepts have been employed to address many medical issues, prepare better delivery systems, and to overcome drug cancer resistance mechanisms.[14–20] Semiconductor nanoparticles ("quantum dots") are proposed as new modalities for fluorescence-based diagnostics and photodynamic therapy.[21] Antibodies improve absorption of gold nanoparticles in cancer cells and were proposed as new image-based diagnostics and photo-thermal therapies.[22,23] All cells have specific proteins on their membranes, which enable recognition and specific-based delivery of agents into the cells with great selectivity. Nutrients, covertures, vesicles, and matrixes also enhance delivery and cytotoxicity of the known therapeutic agents.[14,24,25]

Inorganic oxides with radioisotopes have been used since 1960s to combine the advantages of both radiotherapy and embolization procedures: they are denser and sediment closer to the spot where applied.[26,27] Resins as matrix for radiopharmaceuticals are lighter, and so distribute better in tissues.[28,29] Yttrium-90 is the most used beta particles source to prepare these internal radiotherapy materials, which are injected in main arteries that supply blood to cancer tissues.[30–32] Among advantages of using it in such manner are controlled and higher radiation dose which is locally administrated, which causes less damage to surrounding healthy tissues. It can be preferred to chemotherapeutic agents with similar efficiency for procedures of monitoring and acquiring images because of the less collateral effects, and even to avoid a risky surgery. Nevertheless, there is a need to develop and design better delivery systems for all radiotherapy agents. Radiation delivery systems and embolization might be either pure materials or compound-loaded solid matrixes with particle sizes not greater than 20 µm as not to block hepatic microcirculation.[33] Also, it is important to say that X-ray computed tomography allows visualization of catheters in real time to deliver particles during procedures of internal radiotherapy.[34,35]

Many recent researches use holmium-166 as beta particles source. This rare earth forms stable complexes with many ligands.[36–41] Beta emissions of $^{166}Ho_{67}$ and $^{90}Y_{39}$ in tissues have ranges of 2.1 and 3.6 mm, respectively, and the treatments using the first one are less aggressive with minor damage on healthy surrounding tissues. Gamma-ray emission of $^{166}Ho_{67}$ has less energy than the one coming from the $^{90}Y_{39}$, but it is more abundant, so a scintigraphy diagnostic of tissues retaining holmium-coordinated compounds has become possible.[42–49] Ho(III) is paramagnetic and replaces its inner sphere waters quickly; thus, this rare earth element can act as contrast agent to acquire magnetic resonance images (MRI) as a substitute for the gadolinium compounds.[50–53] Finally, luminescent emission of this trivalent cation in visible spectra (500–530 nm) allows obtaining images of compounds in samples and in vivo by fluorescence-based techniques.[54,55]

Many inconveniences in the use of oxides and resins as matrixes to produce particles for medical therapies come from their long-time stability in the human body what brings a risk of embolization in healthy organs. Recently, the biodegradable matrixes are being preferred to host radionuclides.[56] Their lower time of stability gives them properties of controlled delivery systems: (1) release time of radionuclides is longer than in free formulations, (2) they maintain plasma concentration for a long time, (3) they also locomote in vivo through physical and/or chemical principles.[57] Radioisotope loaded polymeric

matrixes change their properties with the radioactive decays dose, such as degradation time in vivo. For example, gamma rays may induce radiolysis in polymers during their industrial processing or sterilization or even promote polymerization or cross-linking of matrixes, which depend on polymer nature and radiation dose.[58–67]

An ideal procedure to obtain radiopharmaceuticals at lower costs and in greater amounts involves the development of microdevices loaded with the chosen radionuclide and posterior activation in a nuclear reactor. Emulsification process is commonly used in chemistry, food, and (radio) pharmaceutics due to the nature of the materials that can dissolve or disperse in drops, micelles, or vesicles.[68–71]

Although some disadvantages in obtaining radiopharmaceutical particles involve damage or aggregation during a nuclear activation of radioisotopes in biodegradable polymers matrixes, these materials are extensively used to carry and deliver radiation as they enable an easier absorption by tumors. Many of studied materials are cellular nutrients or substrates for tissue engineering and when used to deliver radiation, cancer cells suffer radiation damages by absorbing those particles.[72,73] One model for the designed microparticle radiopharmaceuticals to the hepatic cancer intern radiotherapy procedure was produced by emulsification/evaporation of solvent, where holmium acetylacetonate was loaded into the poly(L-lactic acid) microspheres.[32,74–82] Acetylacetonate complexes are commonly used to extract and recover metal transition ions due to their stability that provide a suitable retention of the ions.[83–86]

The high cost of poly(L-lactic acid) limits its applications despite its better crystallinity and slower degradation under biological conditions.[87,88] A substitute polyester to prepare microparticle-based biodegradable radiopharmaceuticals is poly(3-hydroxi-butyrate-co-3-hydroxy-valerate), PHB-HV. Poly(hydroxyl-alkanoates) are easily extracted from microorganisms and very much applicable for biotechnological purposes.[89,90] For instance, cultures of the bacteria *Alcaligenis eutrophus* supplied by sugar as a carbon source and in scarcity of nitrogen nutrients produce massively these polyesters like a nutritional stock and if sugar is replaced by the propionic acid, *Alcaligenis eutrophus* produces copolymers of 3-hydroxy-butyrates and 3-hydroxy-valerates instead.[91]

Poly(3-hydroxy-butyrate), PHB is the most studied poly(hydroxyl-alkanoate), although it is a brittle material and inadequate for many industrial and clinical applications; its copolymers or blends with other polyesters

enhance mechanical properties, such as elasticity.[92] Therefore, we prepared holmium acetylacetonate loaded PHB-HV microdevices using raw poly(3-hydroxy-butyrate) with 5% and 8% of 3-hydroxy-valetarate by emulsification/evaporation of solvent. These microparticles were evaluated as potential radiopharmaceutical and contrast agent by T_2 and T_2^* weighted MRI. It is worth saying that holmium acetylacetonate microspheres are known for the latter property.[93]

The transverse relaxation time (T_2) is the decay constant of recovery of xy component or the vector of magnetization of nuclear spin initial or its equilibrium value. Physically, it depends on changes in nuclear spin magnetization: magnetic fields applied in real samples have random and transient changes of the local alignment, and/or own sample may have an intrinsical inhomogeneity; the diffused nuclear spin precession frequency defines a band of radiofrequency absorption. This is an intramolecular interaction caused by spin–spin nuclear and/or electronic events. Large molecules may have an intrinsic magnetic field, but their internal components can affect it easily and reduce T_2 relaxation time; small molecules and free flow water are less disturbed. Lipid rich tissues or muscles have water as a structure material, and T_2 lower than blood water. Convention of T_2 weighted images on magnetic resonance (MR) is that white color represents locals rich in free water.[94] White color indicates sites of greatest T_2 like kidneys, gonads, inflammation, fluid, crystals, protein-rich tissues, and blood derivatives. Tissues which are rich in fats or the spinal lipid portion appear white or gray according to the free water content in the range of T_2 values typical for tissues with more fix water molecules as liver, pancreas, muscle, cartilage, or tissues rich in collagen. Finally, poor water-free tissues such as bone, tissues without water (lungs) and fast-moving fluids exhibit lower T_2, and also water bounded to paramagnetic elements – electronic spin facilitates the nuclear spin relaxation process and, thus, appear black in these images.

Finally, all real systems exchange energy by intermolecular interactions, so the energy is distributed in states denoting rotational, vibrational, electronical, or other energy levels in an atom or a molecule. Different chemical compositions in the environment, such as the presence of coagulum and microparticles and inhomogeneity of applied magnetic field affect the distribution of states. To the nuclear spin precession frequencies, it causes dephasing in T_2 relaxation times and frequencies, and it has a relaxation time constant denoted as T_2^*.[95,96] T_2 and T_2^* weighted images of the holmium acetylacetonate loaded

PHB-HV microspheres were compared to inclusion complexes between holmium acetylacetonate and β-cyclodextrin or hydroxyl-propyl-β-cyclodextrin, because these host-guest systems dissolve in water.[96] At this stage, the obtained materials were not capped by hydrophilic materials, but once other hydrophobic materials easily suffer anchoring by the opsonist, proteins that induce immunological reaction of macrophages, were considered as materials with great possibility to be applied in cancer treatments as they are.[97–99] We focused on 20–53 μm sized particles because of their potential application in hepatic cancer brachytherapy procedures.

Materials and methods
Materials
Holmium chloride hexahydrate, poly(vinyl alcohol) (MM 13,000–23,000 g mol^{-1}, 98% hydrolyzed), poly(3-hydroxy-butyrate-co-3-hydroxy-valerate) (PHB-HV) with 5% or 8% amounts of 3-hydroxy-valerate in copolymer were obtained from the Sigma-Aldrich. Acetylacetonate and chloroform were from Vetec (Brazil). Ammonium hydroxide and nitric acid were obtained from commercial suppliers and used as obtained.

Preparation of holmium acetylacetonate
Holmium acetylacetone was prepared by a modified procedure related by Nijsen et al[82] Acetylacetonate, 225 mL, was dissolved in 1350 mL of water, and pH was adjusted to 8.5 by dropwise addition of concentrated ammonium hydroxide. This solution was stirred for 30 mi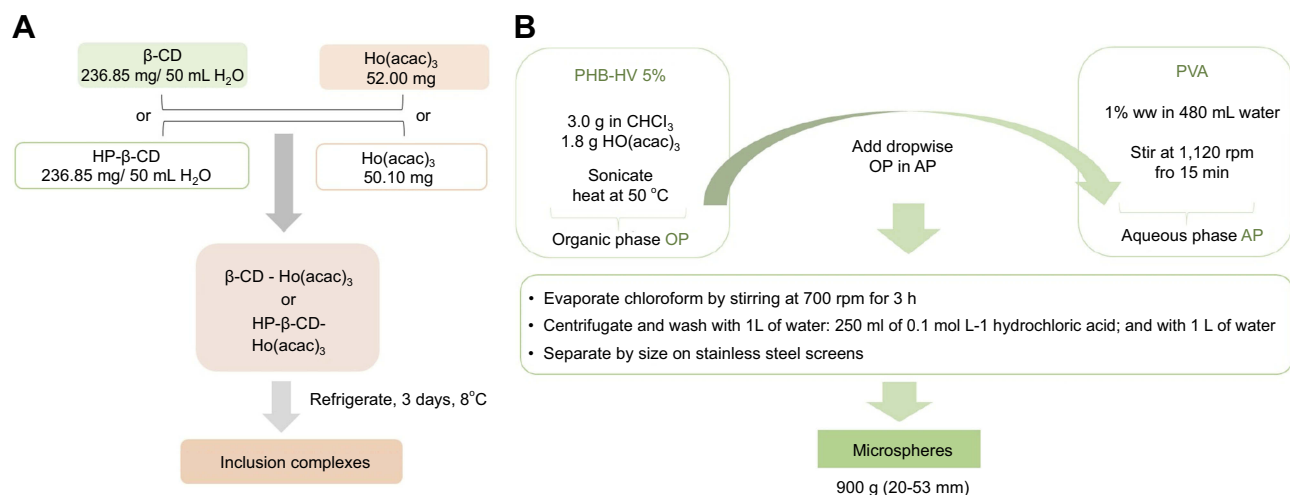ns, and its pH corrected when changed. Holmium chloride hexahydrate (379.38 g mol^{-1}), 9.45 g, was dissolved in 200 mL of water containing 5 drops of concentrated nitric acid and stirred for 2 hrs. HoCl$_3$×6H$_2$O solution was added to the acetylacetone one, and pH was adjusted to 8.5 adding drops of ammonium hydroxide. Reaction continued for 24 hrs under stirring. The orange powder was separated by filtration, washed with water and dried. Mass of 7.0 g (54.4% yield) was obtained and assigned to [Ho(acac)$_3$(H$_2$O)]×2H$_2$O as number of inner sphere water molecules was confirmed by thermogravimetric studies.

Preparation of the β-cyclodextrin-holmium acetylacetonate and the hydroxyl-propyl-β-cyclodextrin inclusion complexes (Scheme 1A)
The inclusion complex between β-cyclodextrin and Ho(acac)$_3$, β-CD-Ho(acac)$_3$ was prepared by dissolving 236.85 mg of β-cyclodextrin in 50.0 mL of water and suspending 52.0 mg of Ho(acac)$_3$ in it, after stirring for 1 hr.[100,101] Then, the suspension was left in the refrigerator for 3 days. Other comparative system was prepared from 277.46 mg of hydroxyl-propyl-β-cyclodextrin (HP-β-CD) and 50.1 mg of Ho(acac)$_3$ using the aforementioned procedure to obtain a new inclusion complex, HP-β-CD-Ho(acac)$_3$.

Emulsification process to prepare PHB-HV microspheres (Scheme 1B)
PHB-HV 5%-MS
Polymer – 3.0 g of poly(3-hydroxy-butyrate) (PHB) was dissolved in 80 mL of chloroform under sonication and

A

β-CD
236.85 mg/ 50 mL H$_2$O

Ho(acac)$_3$
52.00 mg

or — or

HP-β-CD
236.85 mg/ 50 mL H$_2$O

Ho(acac)$_3$
50.10 mg

β-CD - Ho(acac)$_3$
or
HP-β-CD-Ho(acac)$_3$

Refrigerate, 3 days, 8°C

Inclusion complexes

B

PHB-HV 5%

3.0 g in CHCl$_3$
1.8 g HO(acac)$_3$

Sonicate
heat at 50 °C

Organic phase OP

Add dropwise
OP in AP

PVA

1% ww in 480 mL water

Stir at 1,120 rpm
fro 15 min

Aqueous phase AP

- Evaporate chloroform by stirring at 700 rpm for 3 h
- Centrifuge and wash with 1L of water: 250 ml of 0.1 mol L-1 hydrochloric acid; and with 1 L of water
- Separate by size on stainless steel screens

Microspheres

900 g (20-53 mm)

Scheme 1 Schematic illustration of the synthesis of the inclusion compounds in β-cyclodextrins and of the microspheres with PHB-HB. (**A**) Preparation of the β-cyclodextrin-holmium acetylacetonate and the hydroxyl-propyl-β-cyclodextrin inclusion complexes. (**B**) Emulsification process to prepare PHB-HV 5% microspheres. *The PHB-HV 8% microspheres were prepared following the same scheme.

heating at 50°C. This solution was added dropwise into 480 mL of a 1% (w/w) aqueous solution of poly(vinyl alcohol), under the stirring at 1120 rpm for 15 mins. Residual chloroform was removed decreasing the stirring speed to 700 rpm and for additional 3 hrs. The emulsion was centrifuged with 1 L of water, 250 mL of 0.1 mol L^{-1} hydrochloric acid and again with 1 L of water; and filtered using stainless steel sieves. PHB-HV 8% microspheres (20–53 μm) were obtained in 3.5% yield (107.4 g). To prepare Ho(acac)$_3$ loaded PHB-HV 5% microspheres (PHB-HV 5%/Ho(acac)$_3$-MS), 1.8 g of Ho(III) complex was added in the organic phase with polyester, and the procedure was repeated. PHB-HV 5% Ho(III)-loaded microspheres (20–53 μm) were obtained in a yield of 30% (900.5 g) relative to added polyester mass.

PHB-HV 8%-MS

Using the same procedure, by just changing the ratio of HV applied (as illustrated in Scheme 1) microspheres of 20–53 μm in a yield of 22.0% (330.4 g) were obtained. To prepare the Ho(acac)$_3$ loaded PHB-HV 8% microspheres, PHB-HV 8%-Ho(acac)$_3$-MS, 0.9 g of the Ho(III) complex in chloroform with polyester was added, and the procedure was repeated. PHB-HV 8%-Ho(acac)$_3$-MS with diameters of 20–53 μm in a yield of 8.9% (584.0 g) relative to the initial polymer mass used were obtained.

Stability tests in sodium phosphate buffer, pH 7.4

Samples of PHB-HV/Ho(acac)$_3$ microspheres were studied in sodium phosphate buffer at pH 7.4, which corresponds to physiological pH of human blood. Ten glass flasks were separated. One was filled with 50.00 mL of sodium phosphate buffer and used as a blank probe to evaluate sodium contaminants. The microspheres were put into other flasks as indicated in Table 1, and also 50.00 mL of sodium phosphate buffer was added. Each flask was labeled according to the days of experiment (1–9 days) at the room temperature (25°C). Solution was filtered and Ho (III) concentration by inductively coupled plasma (ICP) atomic emission spectroscopy assay was measured. In this study, a theoretical full holmium acetylacetonate radioactive sample would exhibit 0.39% of the initial radioactivity considering the half-life time of holmium-166.

Characterizations

Scanning electron microscopy (SEM) images were acquired in the Philips XL30 Microscope, with JEOL

Table I Amounts of microspheres (MS) used in the stability tests of PHB-HV/Ho(acac)$_3$

Flask	Microspheres mass added (mg) in each flask in starting day of stability test		Days in which microspheres were exposed to sodium phosphate buffer pH 7.4								
	PHB-HV 5%/Ho(acac)$_3$	PHB-HV 8%/Ho(acac)$_3$	1	2	3	4	5	6	7	8	9
1	10.8	11.0	×								
2	10.4	10.6	×	×							
3	10.4	11.1	×	×	×						
4	10.2	10.0	×	×	×	×					
5	10.6	10.1	×	×	×	×	×				
6	10.3	11.0	×	×	×	×	×	×			
7	11.3	10.8	×	×	×	×	×	×	×		
8	10.4	11.0	×	×	×	×	×	×	×	×	
9	10.1	11.1									×

JSM-7401 model to energy-dispersive X-ray (EDS), to gold recovered samples. Also, Tabletop Microscope TM3000 Hitachi Analytical, with resources to acquire EDS from backscattered electrons, samples without covertures, under operating voltage of 15 kV ("Analytical mode") was used.

Infrared spectra were recorded in the Nicolet 6700 with an ATR and BOMEM MB-100 Economical High-Performance FT-IR, dispersing the pulverized samples or micro materials previously dried in stove for 2 days (70°C), in potassium bromide pellets. The spectral range explored was of 400–4000 cm^{-1}.

X-ray diffractograms of pulverized materials were acquired in a Rigaku Miniflex II X-ray diffractometer, using copper as a radiation source (Cu K$_\alpha$ line of 1.541 Å), recorded from 2θ of 0–50° and scan time of 2 s per step of 0.05°.

Confocal laser scanning microscopy images (CLSM) were obtained in a LSM 500 – Carl Zeiss, excitation wavelength of 488 nm, and complexes' fluorescence was detected in 505–530 nm range.

Thermogravimetry experiments were performed in a 2950 TGAHRV5.4A of TA Instruments, under nitrogen atmosphere (10 mL min^{-1}), heating rate of 10°C min^{-1}, and the temperature range of 25–900°C.

Relaxometry characterization: MRI assays

The relaxometry characterization was performed using MRI to determine if the microparticles showed good contrasts in T$_2$ weighted MR images. For this purpose, a phantom was made in a 24-well culture plate containing suspensions of 1 mL PHB-HV microparticles loaded with holmium acetylacetonate, in the following concentrations: 7.7, 5.0, 3.0, 2.0, and 1.0 mg mL^{-1} disperses in 2% of the agarose. The MRIs were acquired in whole-body 3T MRI scanner with a wrist coil (Magnetom Vision®, Siemens, Erlangen, Germany), using the T$_2$ multicontrast turbo-spin echo sequence with a TR of 3000 ms, a TE of 8–256 ms, eight echos, field of view 15.9 × 20.0 cm × cm, matrix 256 × 256, slice thickness 3.0 mm, and flip angle 180°. The signal intensity was measured using a circular and homogeneous region of interesting of 20 mm^2. The T$_2$ of each sample was obtained by adjusting to the decay curve, signal intensity vs TE, with a linear monoexponential algorithm Intensity = C*e$^{-\frac{TE}{T2}}$. The transverse relaxivity value, r$_2$, was determined by the linear least square's adjustment of the slope of the graph 1/T$_2$ vs the concentration of the microparticles. In a similar way, the calculation of r$_1$ value

has performed to determine the efficiency of the contrast agent.

Results and discussion
SEM images and EDS spectra

Figure 1A–F shows PHB-HV 5%-MS SEM images. The microparticles are spherical but slightly wrinkled and show sizes ranging from 20 to 50 μm. The observed morphology of the MS probably indicates the effects of evaporation of residual organic solvent after particle formation and/or inherent crystallization of the polyester. Once the PHB-HV 5% dissolution in chloroform required sonication and heat obtained copolymer showed to be sensible to the amount of chloroform present, for example, higher stirring may speed the solvent evaporation and the polyester may form an irregular surface.

PHB-HV 8%-MS SEM images (Figure 2A–F) display a more wrinkled morphology than the PHB-HV 5%-MS microspheres. Their appearance resembles an exfoliated deformed system with sizes ranging from 20 to 30 μm. Again, this may be associated with a high stirring speed
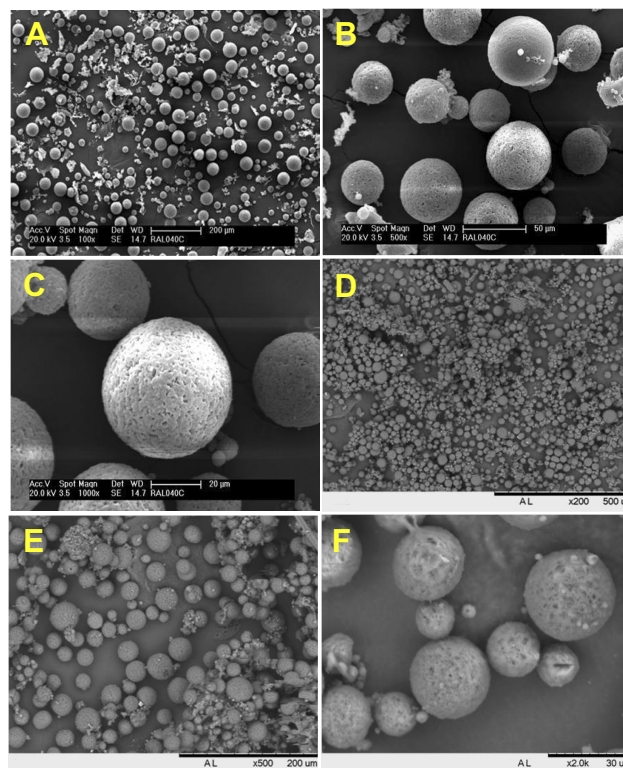
Figure 1 SEM images of PHB-HV 5%-MS in: Philips XL30 Microscope (**A–C**) and Tabletop Microscope TM3000 (**D–F**). Magnifications: (**A**) 100×, (**B**) 500×, (**C**) 1000×, (**D**) 200×, (**E**) 500×, and (**F**) 2000×.
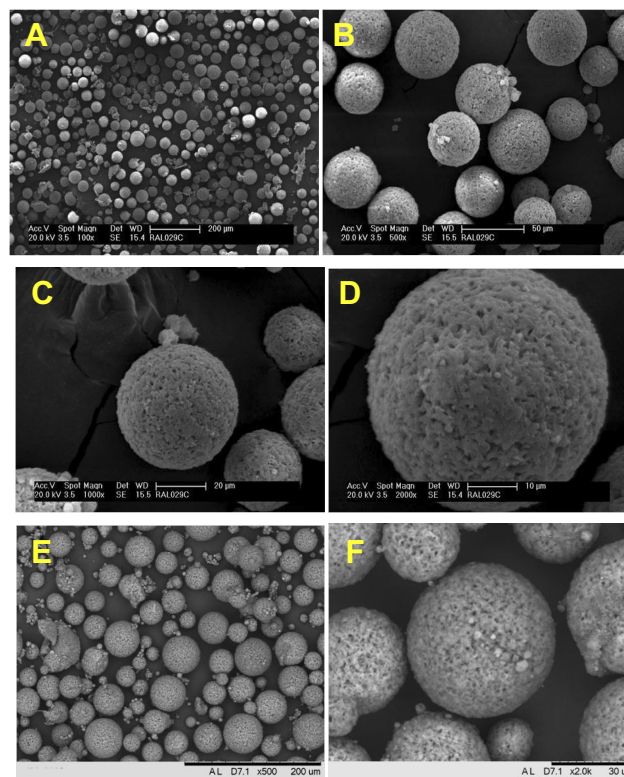**Abbreviations:** SEM, scanning electron microscopy; PHB-HV, poly(3-hydroxi-nutyrate-co-3-hydroxy-valerate); MS, microspheres.
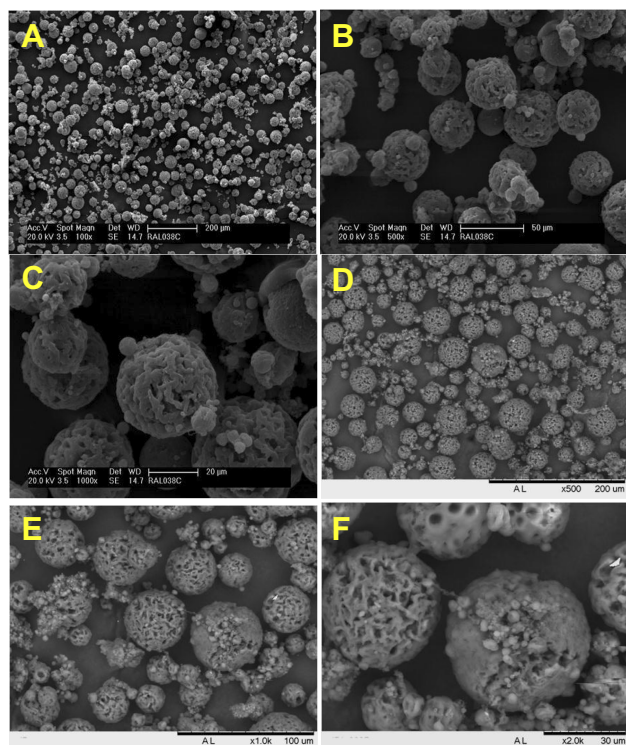
Figure 2 SEM images of PHB-HV 8%-MS in Philips XL30 Microscope (**A–C**) and Tabletop Microscope TM3000 (**D–F**). Magnifications: (**A**) 100×, (**B**) 500×, (**C**) 1000×, (**D**) 500×, (**E**) 1000×, and (**F**) 2000×.
Abbreviations: SEM, scanning electron microscopy; PHB-HV, poly(3-hydroxi-nuty-rate-co-3-hydroxy-valerate); MS, microspheres.

Figure 3 SEM images of the PHB-HV 5%/Ho(acac)$_3$-MS acquired in Philips XL30 Microscope (**A–D**) and Tabletop Microscope TM3000 (**E–F**). Magnifications: (**A**) 100×, (**B**) 500×, (**C**) 1000×, (**D**) 2000×, (**E**) 500×, and (**F**) 2000×.
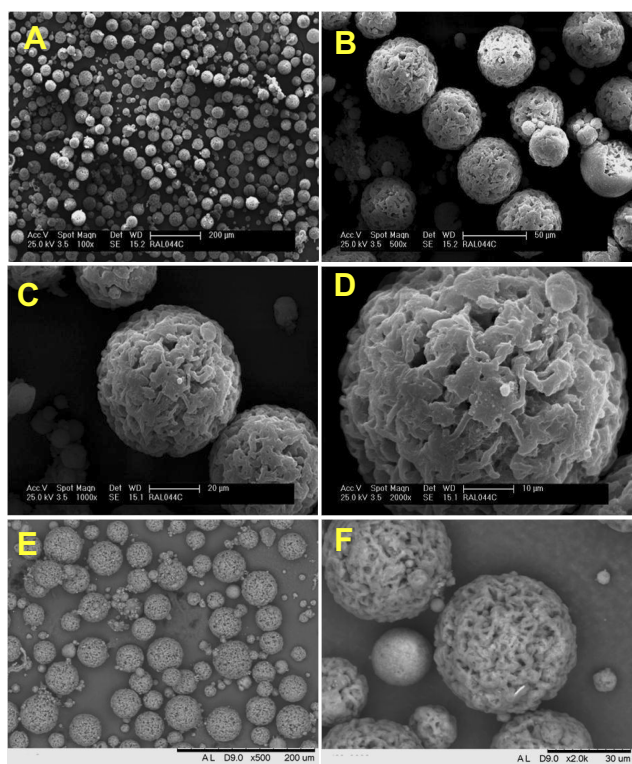**Abbreviations:** SEM, scanning electron microscopy; PHB-HV, poly(3-hydroxi-nuty-rate-co-3-hydroxy-valerate); MS, microspheres.

and fast chloroform removal. Also, this material is some-what more elastic due to the higher amounts of 3-hydroxy-valerate as copolymer.

PHB-HV 5%-Ho(acac)$_3$ -MS SEM images in Figure 3A–F show more spherical microspheres with a smoother surface and with smaller pore sizes than the observed for HB-HV 5%-MS (Figure 1A–F). PHB-HV 5%-Ho(acac)$_3$ -MS showed sizes ranging from 20 to 40 μm. Therefore, it is proposed that holmium acetylacetonate added up some plasticizer property to this copolymer.Figure 2A–F).

In PHB-HV 8%-Ho(acac)$_3$-MS images (Figure 4A–F) similar morphology changes were noted: microspheres had less defects and were more compact with sizes ranging from 40 to 50 μm. These might indicate that the Ho(III) complex was accumulated on the external parts of the microspheres, once the Ho(III) complex aspect seen by SEM images (Figure 5A and B) was in form of the elongated plates.

In both microspheres the EDS spectra were acquired, Figure 6A and B, which also confirmed the presence of Ho(acac)$_3$ loading, judging by the appearance of intense and typical peaks.

CLSM images

The typical green fluorescence of Ho(III)[102] is homoge-neously dispersed in PHB-HV 5%/Ho(acac)$_3$-MS micro-spheres (Figure 7A and B), so it is deduced that the complex is perfectly mixed inside the polyester matrix. Darker microparticles in the lower portion of the images are out of focus materials in the scanning process. However, in PHB-HV 8%/Ho(acac)$_3$-MS (Figure 7C and D), the typical Ho(III) green fluorescence is not continu-ous in greater microspheres and this contradicts their EDS spectral data (Figure 6B). These microparticles displayed the most wrinkled surfaces; thus, it can be assumed that Ho(III) inhomogeneous loading occurred in some parts, or that the irregular layers blocked some of the fluorescence emitted by external parts of these microspheres.

Infrared spectroscopy

The comparative infrared spectra of raw Ho(acac)$_3$ and polyesters and the complex loaded polyester microspheres are shown in Figure 8. The assignment of FT-IR data is shown in Table 2.[103,104] Raw polyesters and the

Figure 4 SEM images of PHB-HV 8%/Ho(acac)$_3$-MS in Philips XL30 Microscope (**A–D**) and Tabletop Microscope TM3000 (**E–F**). Magnifications: (**A**) 100×, (**B**) 500×, (**C**) 1000×, (**D**) 2000×, (**E**) 500×, and (**F**) 2000×.
Abbreviations: SEM, scanning electron microscopy; PHB-HV, poly(3-hydroxi-nutyrate-co-3-hydroxy-valerate); MS, microspheres.
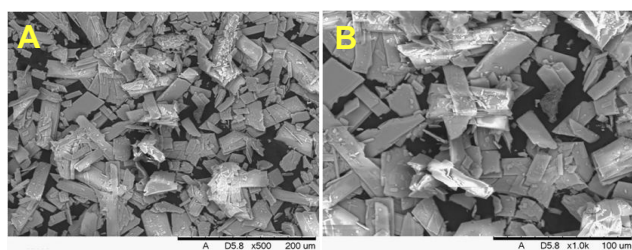
Figure 5 SEM images of Ho(acac)$_3$×3H$_2$O in Tabletop Microscope TM3000. Magnifications: (**A**) 500× and (**B**) 1000×.
Abbreviation: SEM, scanning electron microscopy.

corresponding microparticles FT-IR spectra are quite similar. However, microspheres loaded with Ho(III) showed some characteristic modes of holmium acetylacetonate.

Comparing normal modes of raw PHB-HV 5% and 8%, the only distinction observed was in v(C=O) wavenumber, which showed higher energies for the polyester with 8% of 3-hydroxy-valerate (Table 2, Figure 8). This might have occurred because of packing effects in accordance with the dimensions of the unit cells (obtained by XRD studies, item 4.4). For the PHB-HV 5%/Ho(acac)$_3$-

MS, it was seen that one v(C–H) band had higher energy that might be associated to steric influences of loaded material on the aliphatic portions of copolymer. Thus, an expressive amount of complex inside the copolymer matrix might had provoked the observed shift. Both microspheres infrared spectra indicate coordination of acetylacetonate and Ho(III) by enol tautomer (1600 cm^{-1}- v (C=O)) and 1520 cm^{-1} (v(C=C)). Another indicative for a great loading of complex in the PHB-HV 5%/Ho(acac)$_3$-MS could be associated with weaker bands of Ho(acac)$_3$ assigned as π(C-H) near 760 cm^{-1}, and v(Ho-O) around 490 cm^{-1} and 648 cm^{-1}.

X-ray diffraction (XRD) data

XRD of the two raw PHB-HV (Figure 9A) materials revealed crystallinity of these materials in short and medium distances, observed through intense peaks in 2θ =13.3° and 16.7°. Some long-range ordering by peaks at 2θ=20–22° could be attributed to preserved tendency in their respective Ho(acac)$_3$ loaded microspheres. Typical peaks and crystalline planes of poly(3-hydroxy-butyrate) PHB are: 13.5° (020), 16.9° (110), 20.0° (021), 21.5° (101), 22.4° (111), 25.6° (121), and 27.2° (040).[105] Once they were noted in the copolymers, the amount of 3-hydroxy-valerate did not affect crystallization of main polyester – PHB. However, in PHB-HV 8% microspheres (MS), these peaks were more shifted to lower 2θ values than in PHB-HV 5% MS, so 3-hydroxy-valerate gave more elasticity to polyester and defined crystallinity in a more compact manner, as already proposed in assignments of v(C=O) of this material.

The PHB-HV 8%/Ho(acac)$_3$-MS XRD was quite similar to PHB-HV 8% (Figure 9B). Small loss of intensity could be attributed to: (1) holmium acetylacetonate loading that interacted with polymer as plasticizer, and therefore part of polyester became amorphous, or (2) possible effect caused by emulsification. Polyester and Ho(III) loaded microspheres showed very similar peaks at 21.44° and 22.28°. Nevertheless, the peak at 21.76° lost definition and resolution in microspheres with Ho(III). This might suggest a decrease of crystallinity and structural change. Peaks above 30° were displaced to lower 2θ, what might be indicative for better packing in presence of Ho(acac)$_3$. Despite all, none of the characteristic peaks of holmium acetylacetonate were noted in XRD illustrated in Figure 9B, neither as a crystalline system (Figure 9C) or a more amorphous one (Figure 9D) which could reveal quite a
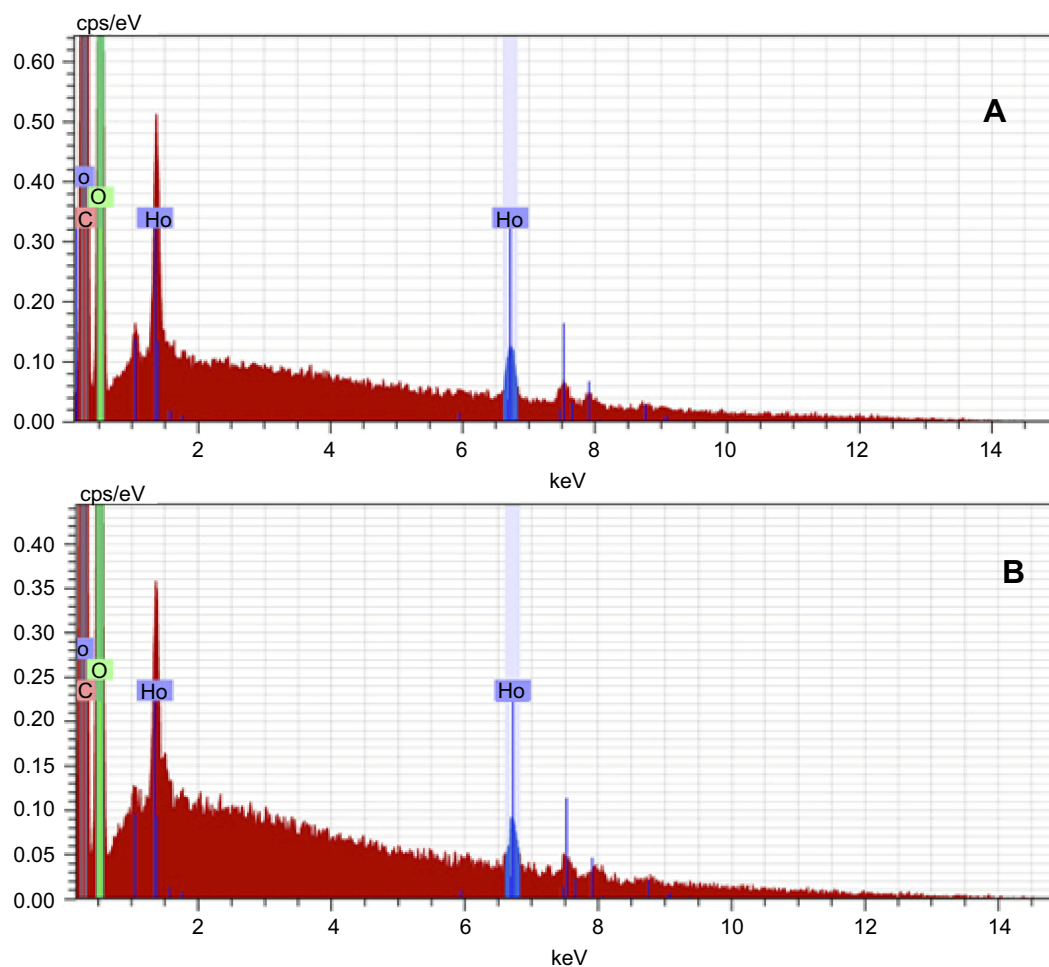
Figure 6 The EDS spectra of (**A**) PHB-HV 5%/Ho(acac)$_3$-MS; and (**B**) PHB-HV8%/Ho(acac)3-MS, both acquired in Tabletop Microscope TM3000.
Abbreviatons: EDS, energy-disperSive x-ray; PHB-HV, poly(3-hydroxi-nutyrate-co-3-hydroxy-valerate); MS, microspheres.

small loading in terms of weight of Ho(III) in the microspheres.

In PHB-HV 5%/Ho(acac)$_3$-MS XRD (Figure 9B), an expressive loss of XRD intensity of polyester peaks in relation to the raw material (Figure 9A) was observed, indicating that the complex loading was high enough to disturb crystallization of organic matrix. Mostly, this could not be attributed to a simple effect of emulsification, because a new and broad peak at 6.48° (Figure 9B) is seen, similar to the most intense peak of Ho(acac)$_3$ in an amorphous condition (Figure 9D). It could be related also to some loss of luminescence in the PHB-HV 5%/Ho (acac)$_3$-MS bigger microspheres previously shown in Figure 7A and B. Probably, acetylacetonate was not linked to Ho(III) in an ideal geometry and could not induce strong antenna effect nor enhance Ho(III) fluorescence.

Using Bragg's Law equation, 2θ diffraction angles were converted into interplanar distances, which could be related to the Miller indices (hkl) and, finally, unit cell parameters (abc): in orthorhombic cell, the diffraction planes were related to hkl indices by Equation 1. It was also possible to calculate the polyesters' crystallinities by Sherrer formula in Equation 2.

$$d = \left[\left(h^2/a^2\right) + \left(k^2/b^2\right) + \left(l^2/c^2\right)\right]^{-1/2} \quad (1)$$

$$T = 0.9\lambda/(Bcos\theta_B) \quad (2)$$

We have used the planes 020 (13.5°), 110 (16.9°), and 021 (20.0°) as intense peaks, unaffected by Ho(III) load. Poly(3-hydroxy-butyrate) unit cell parameters were: a =5.69 Å, b =13.04 Å, and c =5.90 Å.[106] The peak related to the plane 110 at 16.72° was used as reference to determine average sizes of crystallites using the Sherrer formula. The results are summarized in Table 3.

The PHB-HV unit cell was revealed to be slightly larger than that of PHB because of steric hindrance. In
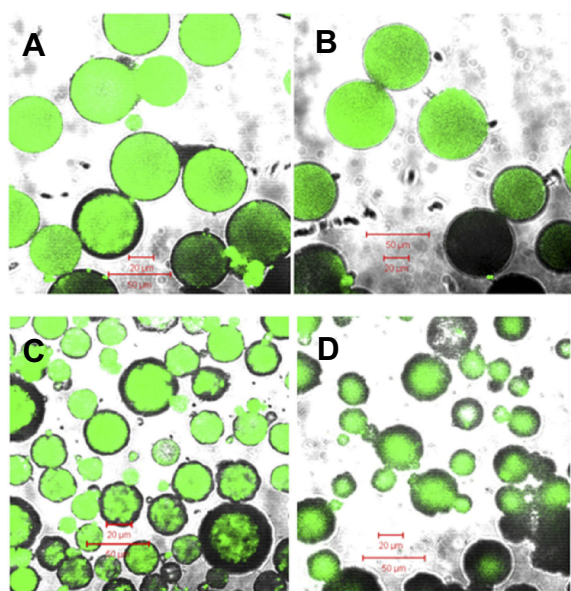
Figure 7 CLSM images of: (**A** and **B**) PHB-HV 5%/Ho(acac)₃-MS; and (**C** and **D**) PHB-HV 8%/Ho(acac)3-MS.
Abbreviations: CLSM, confocal laser scanning microscopy; PHB-HV, poly(3-hydroxi-butyrate-co-3-hydroxy-valerate); MS, microspheres.

PHB-HV 5%/Ho(acac)₃-MS parameters (Table 3) it was noted a slight increase in 00l and 0k0 directions related to PHB-HV 5%, which did not occur in PHB-HV 8%/Ho (acac)₃-MS. This is consistent with discussion based on XRD data and relation between peak intensity and Ho(III) load. Again, it is proposed a high holmium acetylacetonate load in PHB-HV 5%/Ho(acac)₃-MS, mainly following kl direction. In PHB-HV 8%/Ho(acac)₃-MS, unit cells' parameters exhibited a slight shortening in h direction and large increase in l one: despite a low Ho(III) load, its plasticizing effect was noted, a fact that might justify the particles' smoother surfaces seen in Figure 4A–F.

Finally, comparing unit cells' parameters of PHB-HV 5% or 8%, it was noted that the last polymer cell was shorter in 001 direction. This might be explained by a low complex loading, for example, if the 001 direction is important – when copolymer crystallites are smaller, they are less affected by any distortion or poor crystallization and leave enough room for the insertion of holmium acetylacetonate. On the other hand, PHB-HV 5%/Ho (acac)₃-MS showed larger cell parameter in y plane (direction 0k0), therefore, this direction is proposed as preferential one for Ho(III) insertion.

Thermogravimetry

This method was used to quantify holmium acetylacetonate loading in PHB-HV/Ho(acac)₃-MS. To identify the sequence of Ho(acac)₃ thermal decomposition events, an analogy to lanthanum acetylacetonate study was explored.[106,107]
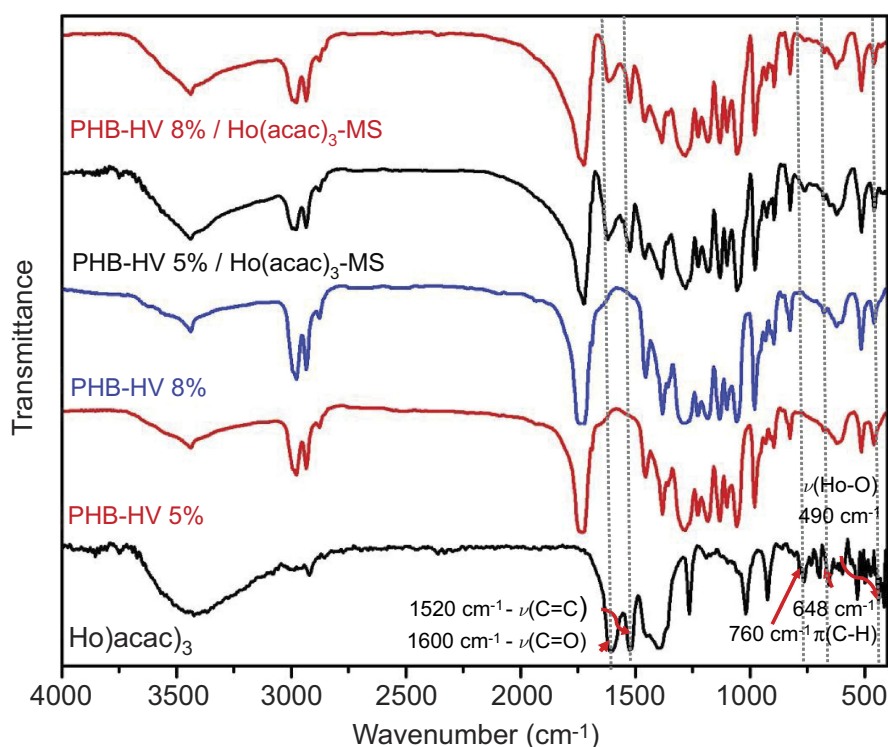
Figure 8 Infrared spectra of raw materials, polyesters, and micromaterials.

Table 2 Assignments of normal modes to raw Ho(acac)$_3$, polyesters, and to microspheres (MS)

| Ho(acac)$_3$ cm^{-1}	PHB-HV 5% cm^{-1}	PHB-HV 8% cm^{-1}	PHB-HV 5%/ Ho(acac)$_3$ cm^{-1}	PHB-HV 8%/Ho(acac)$_3$ cm^{-1}	Assignments
3421	3437	3437	3437	3437	ν(O–H)
2997	2977	2978	2997	2977	ν(C–H)$_{asym}$
2966					ν(C–H)$_{asym}$
2924	2935	2935	2935	2935	ν(C–H)$_{asym}$
	2877	2877	2877	2877	ν(C–H)$_{sym}$
	1728	1736	1724	1724	ν(C=O) carboxylic
1605			1620	1616	ν(C=O) enol
1524			1524	1524	ν(C=C)
1450	1454	1454	1458	1458	δ(C-H)$_{op,\ asym}$
1396					ν(C=O)+ν(C=C)
	1381	1381	1385	1385	δ(C–H)$_{ip,\ sym}$
	1358	1358	1362	1358	δ(C–H)$_{ip,\ sym}$
	1281	1281	1281	1281	ν(C–C–O)$_{asym}$
1265					ν(C=O)+ν(C–CH$_3$)
	1227	1227	1227	1227	ω(CH$_2$)
1192					ν(C–O)
	1184	1184	1180	1184	ω(CH$_2$)
	1134	1134	1130	1130	ω(CH$_2$)
	1099	1099	1099	1099	ω(CH$_2$)
	1057	1057	1057	1057	ν(O–CH$_2$–C)$_{asym}$
1018					ρ(CH$_3$)+ν(C=O)
	980	980	980	980	ν(CHOH–CH$_3$)+ ω(CH$_2$)
	933	933		930	ν(CHOH–CH$_3$)
922	910	910	910		ν(C–CH$_3$)
	895	895	895	895	ν(C–C–O)$_{inp}$
	825	825	825	825	τ(CH$_2$)
764			760		π(C–H)
698					π(C–H)
	675	679	675	679	δ(O–H)$_{outp}$
656			648		ν(C–CH$_3$)+ν(Ho–O)
	621	621	621	621	ω(C=O)
602					ω(C=O) enol
536					δ(O=C–CH$_3$)
	513	517	513	513	
494			486		ν(Ho–O)
474					ν(Ho–O)
	459	459	459	459	ν(Ho–O)
424			420	428	δ(C=C–CH$_3$)

Abbreviations: op, out of phase mode; ip, in phase mode; inp, in plane mode; outp, out plane mode; ν, stretching; δ, in plane bending; ρ, "rocking" deformation; ω, "wagging" deformation; τ, "twist" deformation; "sym", symmetric mode; "asym", asymmetric.

Propyne (C$_3$H$_4$) is released from acetylacetonates in a thermal event. Theoretical sequence for Ho(acac)$_3$ decomposition is proposed in Table 4. It was possible to identify inorganic residue after full decomposition of polyester of microspheres; in PHB-HV this occurred around 330°C.[108]

The thermogravimetric curve and the first derivate for Ho(acac)$_3$ (Figure 10A) were split into events separated by the blue lines, and the determined percentages of residual matter were: (1) 93.08%, (2) 89.47%, (3) 74.21%, (4) 66.50%, (5) 60.75%, and 49.82%.

It was proposed that after first two mass loss events – Ho(acac)$_3$ was fully dehydrated, because of the similarity between theoretical percentage of mass residue calculated in Table 4 (89.53% to event II) and experimental one (89.47%). However, the water molecules release order, as could be modeled by the experimental curve, was of two water
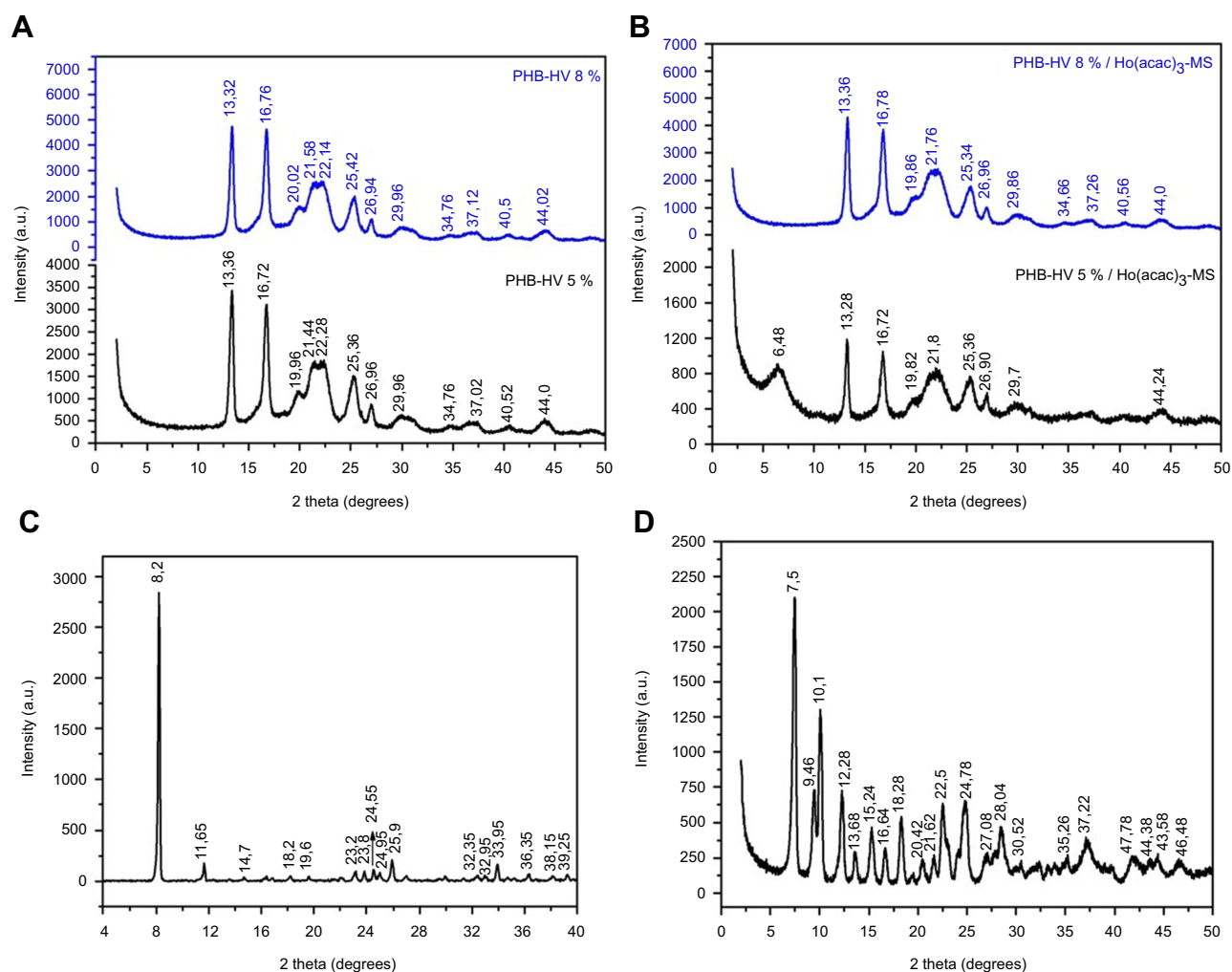
Figure 9 X-ray diffractograms of: (**A**) raw PHB-HV, (**B**) PHB-HV loaded with Ho(acac)$_3$-MS, (**C**) Ho(acac)$_3$-crystalline, and (**D**) Ho(acac)$_3$-amorphous.
Abbreviations: PHB-HV, poly(3-hydroxi-butyrate-co-3-hydroxy-valerate); MS, microspheres.

Table 3 Unit cell parameters of PHB-HV and PHB-HV loaded with Ho(acac)$_3$ microspheres (MS)

Material	2θ (hkl)	Unit cell parameters			Crystallite size (Å)
		a (Å)	b (Å)	c (Å)	
PHB-HV 5%	13.36°, 16.72°, 19.6° (020), (110), (021)	5.79	13.28	6.01	158.95
PHB-HV 5%/Ho(acac)$_3$	13.26°, 16.72°, 19.82° (020), (110), (021)	5.79	13.40	6.03	152.84
PHB-HV 8%	13.32°, 16.76°, 20.02° (020), (110), (021)	5.79	13.28	5.94	155.84
PHB-HV 8%/Ho(acac)$_3$	13.36°, 16.78°, 19.86° (020), (110), (021)	5.75	13.28	6.07	155.84

molecules in the event I (Figure 10A – under average temperature of 92.46°C) rather than one molecule based in predictions the structure resolved by *Koojiman* et al.[109] Ho (III) inner sphere is therefore composed of two water

Table 4 Thermal events proposed and residual mass percentage to $Ho(acac)_3 \times 3H_2O$ thermogravimetry

Thermal event	Theoretical percentage of residual mass
$Ho(acac)_3 \times 3H_2O \rightarrow Ho(acac)_3 \times 2H_2O$ (I – elimination of hydration water)	$[498.29 \text{ g mol}^{-1}/516.30 \text{ g mol}^{-1}] \times 100\% = 96.51\%$
$Ho(acac)_3 \times 2H_2O \rightarrow Ho(acac)_3$ (II – elimination of inner sphere water molecules)	$[462.26 \text{ g mol}^{-1}/516.30 \text{ g mol}^{-1}] \times 100\% = 89.53\%$
$Ho(acac)_3 \rightarrow Ho(CH_3COO)(acac)_2 + C_3H_4$ (III – first release of propyne)	$[422.19 \text{ g mol}^{-1}/516.30 \text{ g mol}^{-1}] \times 100\% = 81.77\%$
$Ho(CH_3COO)(acac)_2 \rightarrow Ho(CH_3COO)_2(acac) + C_3H_4$ (IV – second release of propyne)	$[382.13 \text{ g mol}^{-1}/516.30 \text{ g mol}^{-1}] \times 100\% = 74.01\%$
$Ho(CH_3COO)_2(acac) \rightarrow Ho(CH_3COO)_3 + C_3H_4$ (V – holmium acetate formation)	$[342.06 \text{ g mol}^{-1}/516.30 \text{ g mol}^{-1}] \times 100\% = 66.25\%$
$2Ho(CH_3COO)_3 \rightarrow Ho_2(CO_3)_3 + 3CH_3COCH_3$ (VI – holmium carbonate formation)	$[509.89 \text{ g mol}^{-1}/(2,516.30 \text{ g mol}^{-1})] \times 100\% = 49.38\%$
$Ho_2(CO_3)_3 \rightarrow Ho_2O_2CO_3$ (VII – holmium oxycarbonate formation)	$[421.87 \text{ gmol}^{-1}/(2,516.30 \text{ g mol}^{-1})] \times 100\% = 40.86\%$
$Ho_2O_2CO_3 \rightarrow Ho_2O_3 + CO_2$ (VIII – holmium oxide formation)	$[377.86 \text{ g mol}^{-1}/(2,516.30 \text{ g mol}^{-1})] \times 100\% = 36.59\%$

molecules. This assignment explored the following calculation for complex with molar mass when 1 and 3 waters were present, respectively, 480.27 and 516.30 g mol^{-1}. If we compare the theoretical value for residual mass of (480.27 g mol^{-1}/ 516.30 g mol^{-1}) × 100% = 93.01%, with the one observed in event I (93.08%), two water molecules must be a part of the structure. The temperature of event I was lower than the boiling point of pure water, and could indicate that Ho $(acac)_3$ has two outer sphere (hydration) water molecules, and one water in Ho(III) inner sphere, which was lost under 137.29°C (event II in Figure 10A). Finally, the disposition of ligands around Ho(III) is attributed as asymmetric, considering the uncommon seventh point of coordination and the energy split of v(Ho–O) indicated in Table 2.

Following the sequence of thermal events proposed in Table 4, Figure 10A did not exhibit – even in the first derivative of the thermogravimetric curve – a percentage of residual mass indicative for the distinct releases of first and second propynes (events III and IV), but only the sum of both (theoretical residual mass of 74.01%, and experimental one of 74.21%). Thus, a mixed salt was formed with two acetylacetonates coordinated similarly to Ho(III). Their thermal events occurred at an average temperature, and this is consistent to the assignment of infrared spectral data, which revealed more than one energy band to the v (Ho–O), because of more than one type of chemical bond

strength. Third propyne release and conversion of this intermediate salt to holmium acetate (event V in Table 4, theoretical residual mass of 66.25%) – proposed in an average temperature of 282°C (event 4 in Figure 10A, mass residue of 66.50%) – was observed due to the changes in the first derivative of the thermogravimetric curve, although it was partially hidden by the former thermal event.

The event 5 in Figure 10A is unexpected following the analogies to the $Ln(acac)_3$ in Table 4, since no chemical transformation could provide an experimental mass residue of 60.75%. Compound related is assigned as a mixed salt intermediate $Ho(CH_3COO)_4(CO_3)$ molar mass of 626.05 g mol^{-1} by the following calculation: [626.05 g mol^{-1}/(2 × 516.32 g mol^{-1})] × 100% = 60.63%. Again, two acetates have chemical bonds to the rare earth ion similar in strength, just as predicted for the original two acetylacetonates of the initial complex.

Once all thermal events were characterized, the minimal formula of $Ho(acac)_3$ is assigned as $[Ho(acac)_3 \times (H_2O)] \times 2H_2O$, and the percentage of residual mass to event 6 of Figure 10A, 49.82%, corresponds to 96.1% of the total conversion of this salt to holmium carbonate (event VI in Table 2).

In both PHB-HV/$Ho(acac)_3$–MS thermogravimetry, Figure 10B and C, there was no mass loss around
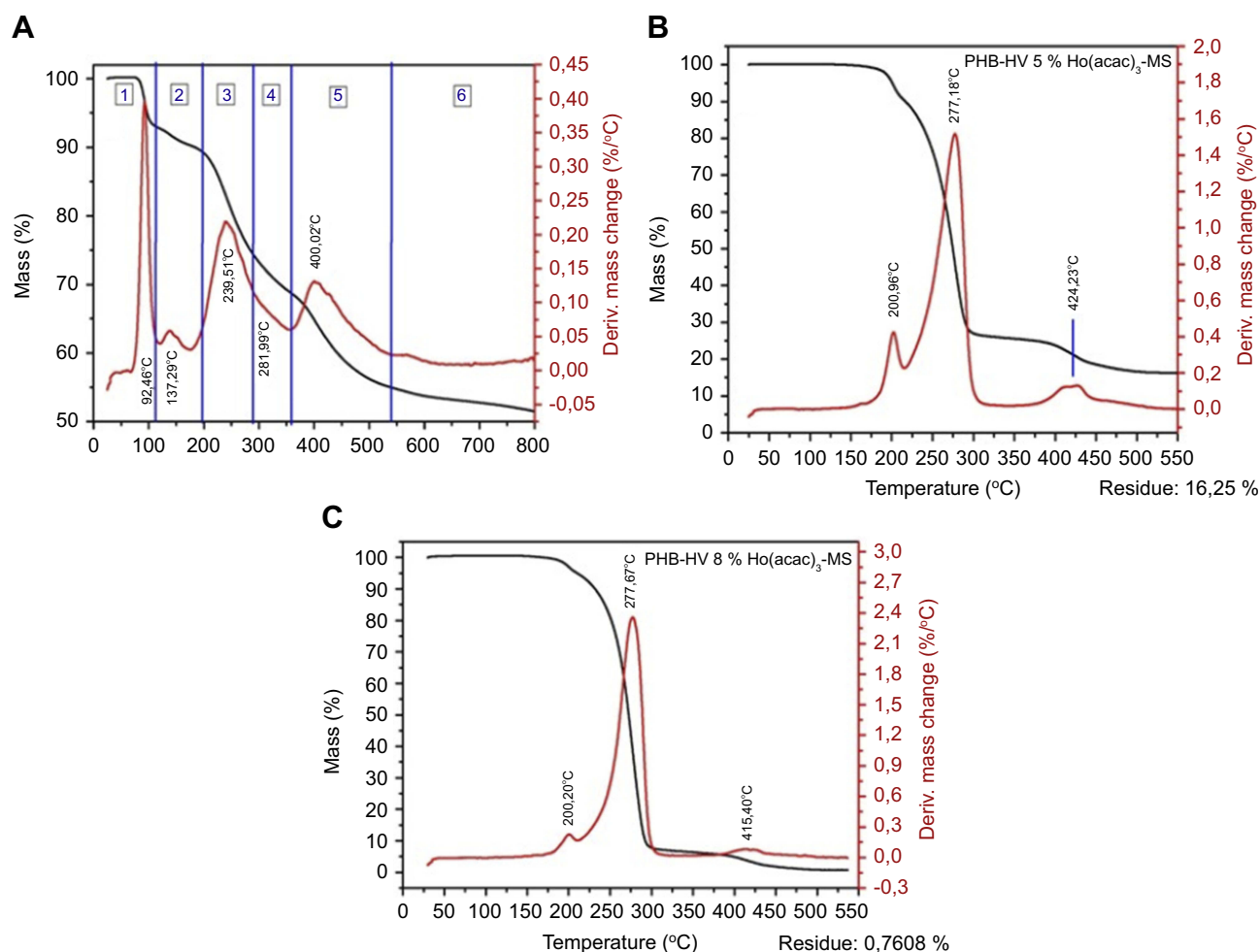
Figure 10 Thermogravimetric curves and their first derivatives obtained for: (**A**) raw Ho(acac)₃; (**B**) PHB-HV 5%/Ho(acac)₃-MS; (**C**) PHB-HV 8%/Ho(acac)₃-MS.
Abbreviations: PHB-HV, poly(3-hydroxi-butyrate-co-3-hydroxy-valerate); MS, microspheres.

100°C, excluding the possibility of adsorbed or hydration water molecules in particles. The first mass loss in these microspheres occurred at an average temperature of 200°C, which did not correspond to poly(vinyl alcohol) degradation: the main event was at 300°C, and an additional one at 400°C could be noted.[110] However, as indicated in Table 3, the infrared spectra of these materials did not reveal an expressive band denoting a considerable amount of this polymer. Hence, the mass losses are assigned to PHB-HV degradation, independent of the 3-hydroxy-valerate amounts, at an average temperature of 277°C (Figure 10B and C). And the thermal events at 201°C and 415–425°C were assigned to holmium acetylacetonate degradation, although the process at 200°C certainly included some matrix degradation. Absence of mass loss of hydration (< 100°C) and crystallization waters (commonly between 100°C and 200°C) accounted

for a replacement of these molecules in the Ho(III) inner sphere by carbonyl and/or carboxyl residues of copolymer, especially in PHB-HV 5%. Hence, the physical or chemical interaction did not induce strong steric consequences to the system.

For PHB-HV 8%/Ho(acac)₃, the percentage of mass residue was so small that the complex loading could not be analyzed according to thermal events of raw complex analogies. Peaks in the first derivative were under temperatures of 239°C and 400°C. However, the complex must be quantified as dehydrated material: there were no hydration or crystallization water molecules. Above 400°C, the salt $Ho_2(CH_3COO)_4(CO_3)$ was formed and maintained as a stable material because the first derivative was constant. Based on this, complex loading was calculated as 0.76% (2 × 462.26 g mol⁻¹)/626.05 g mol⁻¹) = 1.12% in mass. It is interesting that the infrared spectrum

of PHB-HV 8%/Ho(acac)$_3$-MS (Figure 8) exhibited enol normal modes (Table 2) so as the data shown in Figure 6B, which displayed characteristic absorption of holmium. Most of the data obtained by these techniques are of surface components. This is also consistent with the smoother surface of PHB-HV 8%/Ho(acac)$_3$, where the plasticizing effect of HV was noted.

For the PHB-HV 5%/Ho(acac)$_3$-MS, XRD spectrum in Figure 9D revealed that the complex is amorphous. Hence, many properties including thermal degradation are similar to the raw material. Hence, the same quantification process determined that 16.25% × (2 × 462.26 gmol^{-1})/626.05 gmol^{-1}) = 22.15% residual mass. Therefore, PHB-HV 5%/Ho(acac)$_3$-MS are the most promising to the internal radiotherapy aims.

Holmium release essays

Table 5 summarizes the data obtained in the calibration curve for Ho(III) concentration in water observed by ICP. The signal related to sodium phosphate buffer (0 day), and the directed and corrected ICP intensities after discounting the blank read to determine real Ho(III) concentration released by microspheres in ppm. Figure 11A and B illustrate the calibration curve and quantification of Ho(III) according to the number of days that microspheres were exposed to sodium phosphate buffer (pH =7.4).

For all microspheres, the results for stability in the buffer (Table 5) were quite positive: there were no tendencies of a cumulative increase in the concentration of holmium over days under exposure to sodium phosphate buffer (pH 7.4), and Ho(III) concentrations were in the range of 10^{-3} ppm. This could be indicative that under experimental conditions, the release and reuptake of Ho (III) are in a dynamic equilibrium; or simply that the amount of Ho(III) released by microspheres is so low that it is below the detection limit of the equipment. This result opens the possibility of using both kinds of microspheres for medical procedures.

MRI assays

The MR images of the samples dispersed or dissolved in water with agar (Figure 12-I) were acquired according to sample distribution shown in Figure 12-I(**A**), to define a gelatin more solid system in which water is forming chemical bonds with the polysaccharide matrix, becoming somewhat more "structured" due to interactions within itself and with the agar net. The PHB-HV 5%/Ho(acac)$_3$-MS dispersed in a 2% agar revealed a dark phantom as

Table 5 ICP calibration curve and holmium(III) quantification in the sodium phosphate buffer solutions after removing the microparticles, according to days of exposition to sodium phosphate buffer

Calibration curve		Days in buffer	PHB-HV 5%/Ho(acac)$_3$-MS			PHB-HV 8%/Ho(acac)$_3$-MS		
Ho^{+3} (ppm)	ICP (c/s)		ICP (c/s)	[Ho^{+3}] + buffer signal (ppm)	[Ho^{+3}] – buffer signal (ppm)	ICP (c/s)	[Ho^{+3}] + buffer signal (ppm)	[Ho^{+3}] – buffer signal (ppm)
0.00	15.47	0	30.22	0.13504	0	19.47	0.13391	0
2.00	23,293	1	15.39	0.13348	−1.56 × 10^{-3}	17.22	0.13367	−2.40 × 10^{-4}
4.00	38,069	2	16.09	0.13355	−1.49 × 10^{-3}	15.91	0.13353	−3.78 × 10^{-4}
6.00	57,028	3	17.74	0.13372	−1.32 × 10^{-3}	29.29	0.13494	1.03 × 10^{-3}
8.00	77,014	4	48.05	0.13692	1.88 × 10^{-3}	14.54	0.13339	−5.22 × 10^{-4}
10.00	96,903	5	25.38	0.13453	−5.11 × 10^{-4}	29.06	0.13492	1.01 × 10^{-3}
		6	16.42	0.13359	−1.45 × 10^{-3}	20.68	0.13403	1.24 × 10^{-4}
		7	29.86	0.13500	−3.89 × 10^{-5}	13.46	0.13327	−6.36 × 10^{-4}
		8	17.19	0.13367	−1.37 × 10^{-3}	17.25	0.13367	−2.37 × 10^{-4}
		9	45.12	0.13661	1.57 × 10^{-3}	14.63	0.1334	−5.13 × 10^{-4}

A

B
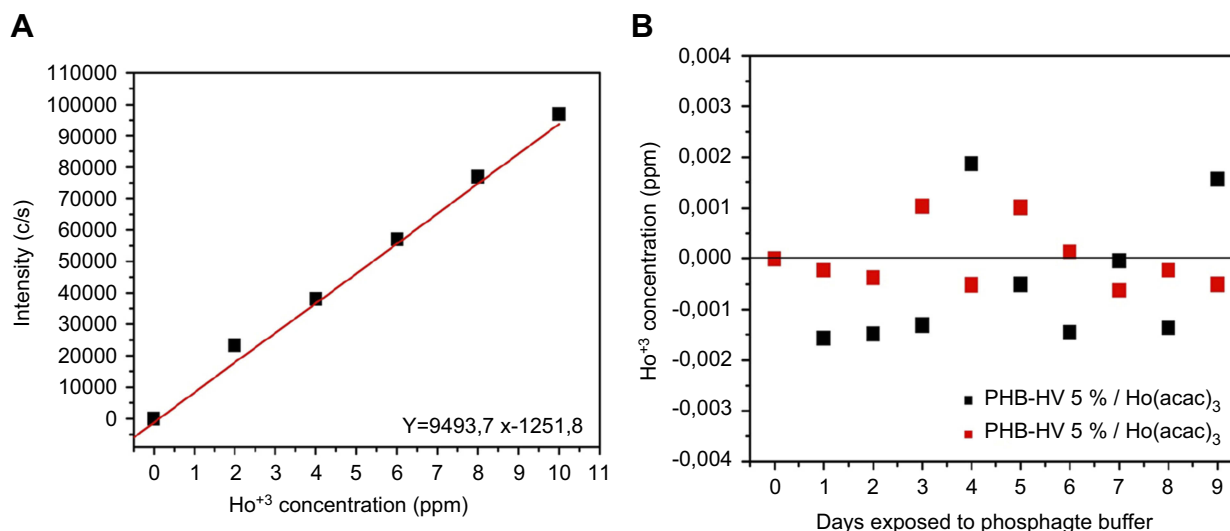
Figure 11 (**A**) Calibration curve to a standard holmium chloride solutions; (**B**) Ho^{+3} concentration in ppm, dosed of the microspheres solutions according to days of exposition to sodium phosphate buffer, pH 7.4.

seen under T$_2$ weighted scan images of protons, Figure 12-I(A1–A5), confirming contrast agent property in this image modality relative to a 2% agar standard. Hence, the paramagnetic nature of the holmium(III) in the wrinkled microspheres affected transverse relaxation time of water, and the darkening is proportional to microsphere (and holmium acetylacetonate) mass present in each sample. Usually, it would be unexpected a T$_2$ relaxation to influence in the water protons caused by lanthanide ions since they usually replace inner sphere waters too fast to affect the nuclear spin relaxation by intermolecular events. But in microspheres, the Ho(III) concentration is much higher, so an expressive part of water molecules is affected by short distance effects to provide better images as shown in Figure 12-I(**B**) A1–A4. Once the paramagnetism of Ho(III) is additive, the whole material had a full magnetic effect comparable to the superparamagnetic nanoparticles with high Fe(III) concentration and provided an intense magnetic field at surface that interacted with water molecules.[111] This result was analogous to the holmium(III) acetylacetonate microspheres reported by Bult et al; but this is the first description of this effect to a complex-loaded PHB-HV matrixes.[93]

The proof of this effect is related to the particle systems and their T$_2$* weighted images illustrated in Figure 12 -I(**C**)A1–A4, which are also darker. It is known that dephasing of spin protons precession frequencies is quicker under the effects of local in homogeneities of the magnetic field. Once the PHB-HV 5%/Ho(acac)$_3$-MS are wrinkled on the surface, the magnetic fields around them

are more complex and multidirectional than in a perfect spherical micromaterial.

Interestingly, the contrast agent effect is also present in the T$_2$ (Figure 12-I(**B**)B1–B2) and T$_2$* (12-I(**C**)B1–B2) weighted scan of the PHB HV 8%/Ho(acac)$_3$-MS, but more mass of microsphere had to be used as to have a similar amount of holmium acetylacetonate in surface interacting with water molecules. This is consistent with the discussion of EDS signal and infrared spectrum signals, so as the contrast agent properties, come from surface elements. On the other hand, it also reveals that in order to produce contrast agent microspheres, only a small load of the holmium acetylacetonate is enough. According to the complex loading, it is possible to prepare an analogous material suitable for MRIs and/or for internal radiotherapeutic purposes, once all the retained PHB-HV/Ho(acac)$_3$-MS in tissues theoretically can be seen by this image technique. Therefore, the elimination of the tumor tissues can be evaluated time by time-lapse observations using the MR images without any injection of other contrast agent, thus, avoiding risks of cumulative toxicity in the period prior to biodegradation of the microparticles.

A final feature is obtained comparing the contrast agent properties of Ho(acac)$_3$ loaded polyester matrixes to Ho (III) inclusion complexes with β-cyclodextrin (Figure 12-I (**C**)C1) or hydroxyl-propyl-β-cyclodextrin, Figure 12-I(**C**) C2. These host-guest systems exhibited the Ho(III) expected contrast in T$_2$ weighted images as they showed white phantom images;[54,96] these inclusion complexes broke spatial ordering of internal water hydrogen bonding
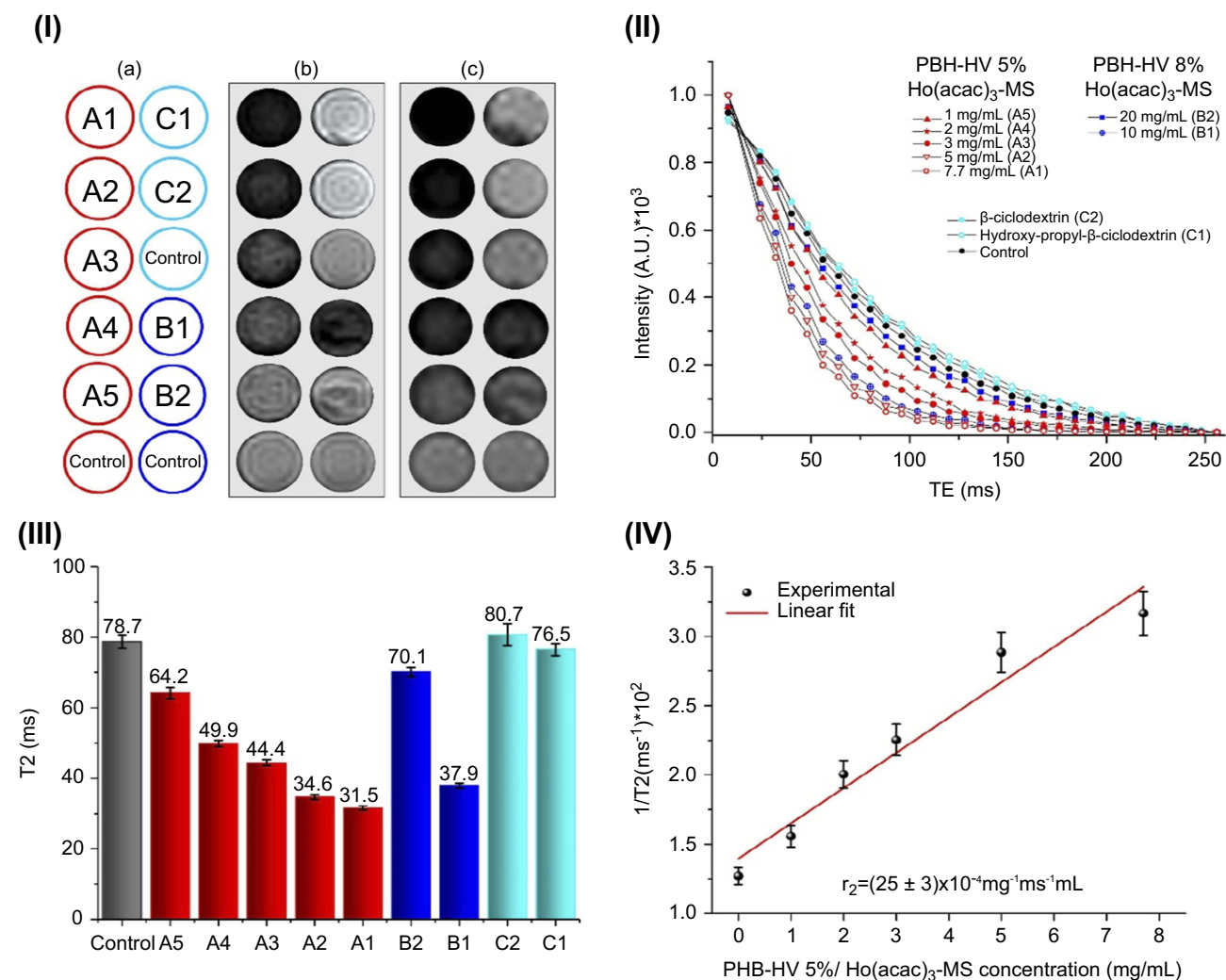
Figure 12 Relaxometry characterization of the PHB-HV microparticles loaded with holmium acetylacetonate. (I) Schematic drawing of samples (A) microsphere added (A1) 7.7 mg; (A2) 5.0 mg; (A3) 3.0 mg; (A4) 2.0 mg; and (A5) 1.0 mg. PHB-HV 8%/Ho(acac)$_3$-MS, mass of microsphere added (B1) 20 mg; (B2) 10 mg. Inclusion complex of β-cyclodextrin and Ho(acac)$_3$, initial concentration of 9.12×10^{-3} mol L^{-1} (C1), and hydroxy-propyl-β-cyclodextrin and Ho(acac)$_3$, initial concentration of 1.94×10^{-3} mol L^{-1} (C1). (B) T$_2$ and (C) T$_2$* weighted MRI of the corresponding samples indicated in (A). (II) Curves of MRI signal intensity of the samples indicated in (A) in the function of TEs. (III) T$_2$ values determined from the curves showed in item (II). (IV) Calculation of the value of r$_2$ from the linear correlation between the inverse of the T$_2$ values of the samples (A1–A5) and the concentrations of the corresponding microparticles.
Abbreviation: PHB-HV, poly(3-hydroxi-nutyrate-co-3-hydroxy-valerate)

and with polysaccharide net as the lanthanide ions quickly replace inner sphere water molecules. However, they are not able to cause a dephasing in protons' spin precession frequencies such as the PHB-HV/Ho(acac)$_3$ microspheres, once their T$_2$* weighted images (Figure 12-I(**C**)C1–C2) had the same color of a 2% agar standard.

To determine the r$_2$, the curves of MRI signal intensity of the samples indicated in (a) in the function of TEs as shown in Figure 12-II were obtained. It was shown that higher microparticle concentrations exhibited lower values of T$_2$ (Figure 12-III). Values for r$_2$ were determined from the linear

correlation between the inverse of the T$_2$ values as follows (shown in Figure 12-IV): T$_2$(A1) = 31.5 ± 0.6 ms, T$_2$ (A2) = 34.6 ± 0.7 ms, T$_2$ (A3) = 44.4 ± 0.9 ms, T$_2$ (A4) = 49.9 ± 0.9 ms, T$_2$ (A5) = 64.2 ± 1.6 ms, and T$_2$ (control) = 78.7 ± 1.9 ms, and the concentrations of the corresponding microparticles, the r$_2$=(25 ±3)× 10^{-4} mg^{-1} ms^{-1} mL and r$_1$=(3.1 ± 0.6) × 10^{-4} mg^{-1} ms^{-1} mL. Taking into account that an MRI contrast agent for T$_2$-weighted images is effective for high values of the r2/r1 ratio, the ratio value of 8.06 obtained, indicate to be an adequate contrast for images T$_2$-weighted for a magnetic field of 3 T magnetic field.[112–114]

Conclusions

The PHB-HV microspheres loaded with holmium(III) acetylacetonate, in which the Ho(III) loading was inversely proportional to the amount of 3-hydroxy-valerate in the copolymer used during the emulsification/evaporation of solvent were successfully produced. The microspheres produced were mostly wrinkled and were loaded with 22% or 12% of Ho(III). Microspheres with higher Ho(III) loading in a PHB copolymer with more poly(3-hydroxy-valerate) 8% were indicated as more suitable to internal radiotherapy procedures. An accumulation of Ho(III) was detected on the surface of these microspheres, and the XRD revealed the preferential direction toward which the Ho(III) complex interacted or simply precipitated in the polyester matrix. No expressive release of Ho(III) was detected in a 9-day exposition period to sodium phosphate buffer (pH 7.4), suggesting the microparticles are highly stable in this simple simulation of the human fluids. Despite the different amounts of holmium (III) acetylacetonate loading, both microspheres proved to be very efficient to obtain T_2 and T_2^* weighted images in the MR. The Ho(III) loaded PHB-HV microspheres showed different properties when compared to the Ho (III) inclusion complexes with β-cyclodextrins. When discussing the cancer tissues diagnostics, either Ho(III) microspheres or host-guest inclusion systems can be used to acquire MR images of patients. Tests with the culture cells and biological fluids, as well as in vivo tests are still being conducted as to reveal the Ho(III) microspheres clinical potential for application and risks.

Nevertheless, this was the first report on the use of inclusion complexes of holmium acetylacetonate in biodegradable polymers as contrast agents, evaluating the endurance of the microparticles under nuclear activation and Ho(III) microsphere use as safer radiopharmaceuticals, although it still needs further testing, we hopefully might have great potential for clinical use.

Abbreviations

CLSM, confocal laser scanning microscopy; EDS, energy-dispersive X-ray; HP-β-CD, hydroxyl-propyl-β-cyclodextrin; Ho(acac)$_3$, holmium(III) acetylacetonate; Ho(acac)$_3$-MS, holmium(III) acetylacetonate microspheres; ICP, inductively coupled plasma; PHB-HV, Poly(3-hydroxi-butyrate-co-3-hydroxy-valerate); MRI, magnetic resonance images; MS, microspheres; PHB, poly(3-hydroxy-butyrate); SEM, scanning electron microscopy; XRD, X-ray diffraction.

Disclosure

The authors report no conflicts of interest in this work.

References

1. Whitesides GM. Nanoscience, nanotechnology, and chemistry. *Small*. 2005;1(2):172–179. doi:10.1002/smll.200400130
2. Xao-Jie C, Xue-Qiong Z, Liu Q, Zhang J, Zhou G. Nanotechnology: a promising method for oral cancer detection and diagnosis. *J Nanobiotechnol*. 2018;16(52):1–17.
3. Capella MAM, Capella LS. A light in muitidrug resistance: photodynamic treatment of muitidrug-resistant tumors. *J Biomed Sci*. 2003;10:361–366. doi:10.1007/bf02256427
4. Schäfer M, Schmitz C, Facius G, et al. Systematic study of parameters influencing the action of Rose Bengal with visible light on bacterial cells: comparison between the biological effect and singlet-oxygen production. *Photochem Photobiol*. 2000;71:514–523.
5. Moraes RM, Dayan FE, Canel C. The lignans of *Podophyllum*. *Stud Nat Prod Chem*. 2002;26(Part G):149–182.
6. You Y. Podophyllotoxin derivatives: current synthetic approaches for new anticancer agents. *Curr Pharm Des*. 2005;11:1695–1717.
7. Rose WC. Preclinical antitumor activity of taxanes, In: *Taxol®-Science and Applications*. Suffness M, editor. chap. 8. CRC Press, Inc.; 1995.
8. Cronstein BN, Montesinos MC, Chan E. Adenosine mediates the antiinflammatory effects of methotrexate as well as its toxicities. *Drug Develop Res*. 2001;52:394–396.
9. Tian H, Cronstein BN. Understanding the mechanisms of action of methotrexate: implications for the treatment of rheumatoid arthritis. *Bull NYH Hosp Jt Dis*. 2007;65(3):168–173.
10. Rosenberg B, Van Camp L, Trosko JE, Mansour VH. Platinum compounds: a new class of potent antitumour agents. *Nature*. 1969;222(5191):385–386. doi:10.1038/222385a0
11. Milenic DE, Brady ED, Brechbiel MW. Antibody targeted radiation cancer therapy. *Nat Rev Drug Discov*. 2004;3(6):488–499. doi:10.1038/nrd1413
12. Lliakis G. The role of DNA double strand breaks in ionizing radiation-induced killing of eukaryotic. *Cells BioEssays*. 1991;13:641–648. doi:10.1002/bies.950131204
13. Kampf G. Induction of DNA double-strand breaks by ionizing radiation of different quality and their relevance for cell inactivation. *Radiobiol Radiother*. 1988;29(6):631–658.
14. Panchapakesan B, Wickstrom E. Nanotechnology for sensing, imaging and treating cancer. *Surg Oncol Clin N Am*. 2007;16:293–305. doi:10.1016/j.soc.2007.03.002
15. Wang MD, Shin DM, Simons JW, Nie S. Nanotechnology for targeted cancer therapy. *Expert Ver Anticancer Ther*. 2007;7:833–837.
16. Shanthill CN, Gupta R, Mahato AK. Traditional and emerging applications of microspheres: a review. *Int J PharmTech Res*. 2010;2(1):675–681.

17. Raguz S, Yagüe E. Resistance to chemotherapy: new treatments and novel insights into an old problem. *Bit J Cancer.* 2008;99:387–391.

18. Luqmani YA. Mechanisms of drug resistance in cancer chemotherapy. *Med Princ Pract.* 2005;14(1):35–48. doi:10.1159/000086183

19. Mellor HR, Callaghan R. Resistance to chemotherapy in cancer: a complex and integrated cellular response. *Pharmacology.* 2008;81:275–300. doi:10.1159/000115967

20. Fojo T. Cancer, DNA repair mechanisms, and resistance to chemotherapy. *J Natl Cancer Inst.* 2001;93(19):1434–1436. doi:10.1093/jnci/93.19.1434

21. Biju V, Itoh T, Anas A, Sujith A, Ishikawa M. Semiconductor quantum dots and metal nanoparticles: syntheses, optical properties, and biological applications. *Anal Bioanal Chem.* 2008;391:2469–2495. doi:10.1007/s00216-008-1856-8

22. EL-Sayed I, Huang X, El-Sayed MA. Surface plasmon resonance scattering and absorption of anti-EGFR antibody conjugated gold nanoparticles in cancer diagnostics: applications in oral cancer. *Nanoletters.* 2005;5(5):829–834.

23. EL-Sayed I, Huang X, El-Sayed MA. Selective laser photo-thermal therapy of epithelial carcinoma using anti-EGFR antibody conjugated gold nanoparticles. *Canc Letters.* 2006;239:129–135.

24. Hamelers IH, Kroon AI. Nanocapsules: a novel lipid formulation platform for platinum-based anti-cancer drugs. *J Liposome Res.* 2007;17(3–4):183–189. doi:10.1080/08982100701530290

25. Grallert SRM, Rangel-Yagui CO, Pasqualoto KFM, Tavares LC. Polymeric micelles and molecular modeling applied to the development of radiopharmaceuticals. *Braz J Pharm Sci.* 2012;48 (1):1–16.

26. LaFave JW, Grotenhuis L, Kim YS, Maclean LD, Perry JF. 90Y-tagged microspheres in adjuvant tumor theraphy. *Surgery.* 1963;53:778–783.

27. Blanchard RJ, Grotenhuis L, LaFave JW, Frye JS, Perry JF. Treatment of experimental tumours. *Arch Surg.* 1964;89:406–409. doi:10.1001/archsurg.1964.01320020170025

28. Kennedy A, Nag S, Salem R, et al. Recommendations for radioembolization of hepatic cancer malignancies using yttrium-90 microsphere brachytherapy: a consensus panel report from the radioembolization brachytherapy oncology consortium. *Int J Radiat Oncol Biol Phys.* 2007;68(1):13–23.

29. Vente MAD, Wondergem M, van der Tweel I, et al. Yttrium-90 microsphere radioembolization for the treatment of liver malignancies: a structured meta-analysis. *Eur Radiol.* 2009;19:951–959.

30. Houle S, Yip TK, Shepherd FA, et al. Hepatocellular carcinoma: pilot trial of treatment with Y-90 microspheres. *Radiology.* 1989;172(3):857–860. doi:10.1148/radiology.172.3.2549567

31. Carr BI, Sheetz M, Brown M, et al. Hepatic arterial ^{90}yttrium-labeled glass microspheres (*Therasphere*) as treatment for unresectable HCC in forty three patients. *Proc Annu Meet Am Assoc Cancer Res.* 2002;21(abstr):553.

32. van Es RJ, Nijsen JF, van Het Schip AD, Dullens HF, Slootweg PJ, Koole R. Intra-arterial embolization of head-and-neck cancer with radioactive holmium-166 poly(L-lactic acid) microspheres: an experimental study in rabbits. *Int J Oral Maxillofac Surg.* 2001;30(5):407–413. doi:10.1054/ijom.2001.0129

33. Vollmar B, Menger MD. The hepatic microcirculation: mechanistic contributions and therapeutic targets in liver injury and repair. *Physiol Rev.* 2009;89:1269–1339. doi:10.1152/physrev.00027.2008

34. Mohnike K, Wieners G, Schwartz F, et al. Computed tomography-guided high-dose brachytherapy in hepatocellular carcinoma: safety, efficacy, and effect on survival. *Int J Radiation Oncology Biol Phys.* 2010;78(1):172–179.

35. Ricke J, Wust P, Wieners G, et al. Liver malignancies: CT-guided interstitial brachytherapy in patients with unfavorable lesions for thermal ablation. *J Vasc Interv Radiol.* 2004;15:1279–1286.

36. Armelao L, Quici S, Barigelletti F, et al. Design of luminescent lanthanide complexes: from molecules to highly efficient photo-emitting materials. *Coord Chem Rev.* 2010;254:487–505.

37. Belian MF, de Sa GF, Alves S Jr, Galembeck A. Systematic study of luminescent properties of new lanthanide complexes using crown ethers as ligand. *J Limun.* 2011;131:856–860.

38. Aiga F, Iwanaga H, Amano A. Density functional theory investigation of Eu(III) complexes with-diketonates and phosphine oxides: model complexes of fluorescence compounds for ultraviolet LED devices. *J Phys Chem A.* 2005;109:11312–11316. doi:10.1021/jp0553535

39. Binnemans K Rare-earth beta-diketonates, In: Gschneider KA Jr, Bünzli JCG, Pecharsky VK, editors. *Handbook on the Physics and Chemistry of Rare Earths*; Vol. 35; Amsterdam: Elsevier; 2003:107–272.

40. Binnemans K, Van Deun R, Görller-Walrand C, et al. Spectroscopic behavior of lanthanide (III) coordination compounds with Schiff base ligands. *Phys Chem Chem Phys.* 2000;2:3753–3757.

41. Pui A, Malutan T, Tataru L, Malutan C, Humelnicu D, Carja G. New complexes of lanthanide Ln (III), (Ln = La, Sm, Gd, Er) with Schiff bases derived from 2-furaldehyde and phenylenediamines. *Polyhedron.* 2011;30:2127–2131.

42. Kim JH, Lee JT, Kim EK, et al. Percutaneous sclerotherapy of renal cysts with a beta-emitting radionuclide, holmium-166-chitosan complex. *Korean J Radiol.* 2004;5:128–133. doi:10.3348/kjr.2004.5.2.128

43. Kheyfits A. Yttrium-90 radioembolization. *Radiol Today.* 2010;11 (9):20.

44. Yttrium-90 handling precautions. Available from: http://www.perkinelmer.com/CMSResources/Images/44-74001tch_yttrium90.pdf. Accessed June 16, 2018.

45. Rajendran JG, Eary JF, Bensinger W, Durack LD, Vernon C, Fritzberg A. High-dose 166Ho-DOTMP in myeloablative treatment of multiple myeloma: pharmacokinetics, biodistribution, and absorbed dose estimation. *J Nucl Med.* 2002;43:1383–1390.

46. Tuner JH, Claringbold PG, Kelmp PBF, et al. 166-Ho microsphere liver radiotherapy: a pre-clinical SPECT dosimetry study in the pig. *Nucl Med Commun.* 1994;15:545–553.

47. Nijsen JFW, Zonnenberg BA, Woittiez JR, et al. Holmium-166 poly lactic acid microspheres applicable for intra-arterial radionuclide therapy of hepatic malignancies: effects of preparation and neutron activation techniques. *Eur J Nucl Med.* 1994;26:699–704.

48. Zielhuis SW, Nijsen JFW, Seenwoolde JH, et al. Long-term toxicity of holmium loaded poly(L-lactic acid) microspheres in rats. *Biomaterials.* 2007;28:4591–4599. doi:10.1016/j.biomaterials.2007.07.012

49. Vente MA, Nijsen JF, de Wit TC, et al. Clinical effects of transcatheter hepatic arterial embolization with holmium-166 poly(L-lactic acid) microspheres in healthy pigs. *Eur J Nucl Med Mol Imaging.* 2008;35:1259–1271. doi:10.1007/s00259-008-0747-8

50. Speenwoolde JH, Nijsen JF, Bartels LW, Zielhus SW, van Het Schip AD, Bakker CJ. Internal radiation therapy of liver tumors: qualitative and quantitative magnetic resonance imaging of the biodistribution of holmium-loaded microspheres in animal models. *Magn Reson Med.* 2004;53:76–84.

51. Norek M, Peters JA. MRI contrast agents based on dysprosium or holmium. *Prog Nucl Mag Res Sp.* 2011;59:64–82.

52. Aime S, Carrera C, Castelli DD, Crich SG, Terreno E. Tunable imaging of cells labeled with MRI-PARACEST agents. *Angew Chim Int Ed.* 2005;44:1813–1815.

53. Caravan P. Strategies for increasing the sensitivity of gadolinium based MRI contrast agents. *Chem Soc Rev.* 2006;35:512–523. doi:10.1039/b510982p

54. Thibon A, Pierre VC. Principles of responsive lanthanide-based luminescent probes for cellular imaging. *Anal Bioanal Chem.* 2009;394:107–120. doi:10.1007/s00216-009-2683-2

55. Bünzli JC. Lanthanide luminescence for biomedical analyses and imaging. *Chem Rev*. 2010;110:2729–2755.

56. Azevedo MBM, Melo VHS, Soares CRJ, et al. Development and characterisation of polymeric microparticle of poly(d,l-lactic acid) loaded with holmium acetylacetonate. *J Microencapsul*. 2018;35 (3):281–291. doi:10.1080/02652048.2018.1477843

57. Swbrick J. *Encyclopedia of Pharmaceutical Technology*. England: Informa Healthcare; 2007.

58. El-Sawy NM, El-Arnaouty MB, Ghaffar AMA. γ-Irradiation effect on the non-cross-linked and cross-linked polyvinyl alcohol films. *Polym Plast Technol Eng*. 2010;49:169–177.

59. Milicevic D, Trifunovic S, Galovic S, Suljovrujic E. Thermal and crystallization behaviour of gamma irradiated PLLA. *Radiat Phys Chem*. 2007;76:1376–1380.

60. Carswell-Pomerantz T, Hill DJT, O'Donnell JH, Pomery PJ. An electron spin resonance study of the radiation chemistry of poly (hydroxybutyrate). *Radiat Phys Chem*. 1995;45:737–744.

61. Luo S, Netravali AN. Effect of 60Co γ-radiation on the properties of poly(hydroxybutyrate-co-hydroxyvalerate). *J Appl Polym Sci*. 1999;73:1059–1067.

62. Choi WS, Ahn KJ, Lee DW, Byun MW, Park HJ. Preparation of chitosan oligomers by irradiation. *Polym Degrad Stabil*. 2002;78:533–538.

63. Gryczka U, Dondi D, Chmielewski AG, Migdal W, Buttafava A, Faucitano A. The mechanism of chitosan degradation by gamma and e-beam irradiation. *Radiat Phys Chem*. 2009;78:543–548.

64. Sato K. Radiation sterilization of medical products. *Radioisotopes*. 1983;32:431–439.

65. Wang B, Kodama M, Mukataka S, Kokufuta E. On the intermolecular crosslinking of PVA chains in an aqueous solution by γ-ray irradiation. *Polym Gels Netw*. 1998;6:71–81.

66. Chang Z, Liu G, Tian Y, Zhang Z. Preparation of micron-size monodisperse poly(vinyl acetate) microspheres with γ-rays-initiated dispersion polymerization in microreactor. *Mater Lett*. 2004;58:522–524.

67. Yang SL, Wu ZH, Yang W, Yang MB. Thermal and mechanical properties of chemical crosslinked polylactide (PLA). *Polym Test*. 2008;27:957–963.

68. Ayyub P, Maitra AN, Shah DO. Formation of theoretical density microhomogeneous Yba2Cu3O7-x, using a microemulsion – mediated process. *Physica C*. 1990;168:571–579.

69. Kumar P, Pillai V, Bates SR, Shah DO. Preparation of Yba2cu3o7-X superconductor by coprecipitation of nanosize oxalate precursor powder in microemulsions. *Mater Lett*. 1993;16(2–3):68–74.

70. Rangasamy M. Nano technology: a review. *J Appl Pharm Sci*. 2011;01(02):08–16.

71. Vieira DB, Gamarra LF. Advances in the use of nanocarriers for cancer diagnosis and treatment. *Einstein* 2016;14:99-103. doi:10.1590/S1679-45082016RB3475 (

72. Armentano I, Dottori M, Fortunati E, Mattioli S, Kenny JM. Biodegradable polymer matrix nanocomposites for tissue engineering: a review. *Polym Degrad Stabil*. 2010;95:2126–2146.

73. Benicewicz BC, Hopper PH. Polymer for absorbable surgical sutures – part II. *J Bioact Compat Polym*. 1991;6:64–94.

74. Mumper RJ, Jay M. Formation and stability of lanthanide complexes and their encapsulation into polymeric microspheres. *J Phys Chem*. 1992;96:8626–8631.

75. Nijsen JFW, van Steenbergen MJ, Kooijiman H, et al. Influence of neutron irradiation on holmium acetylacetonate loaded poly(l-lactic acid) microspheres. *Biomaterials*. 2001;22:3073–3081.

76. Nijsen JFW, van Steenbergen MJ, Kooijiman H, et al. Characterization of poly(L-acid lactic) microspheres loaded with holmium acetylacetonate loaded. *Biomaterials*. 2001;22:3073–3081.

77. Zielhuis SW, Nijsen JFW, Figueiredo F, et al. Surface characteristics of holmium-loaded poly(L-lactic acid) microspheres. *Biomaterials*. 2005;26:925–932. doi:10.1016/j.biomaterials.2004.03.028

78. Zielhuis SW, Nijsen JFW, de Roos R, et al. Production of GMP-grade radioactive holmium loaded poly(l-lactic acid) microspheres for clinical application. *Int J Pharm*. 2006;311:69–74. doi:10.1016/j.ijpharm.2005.12.034

79. Hamoudeh M, Fessi H, Salim H, Barbos D. Holmium-loaded PLLA nanoparticles for intratumoral radiotherapy via the TMT technique: preparation, characterization, and stability evaluation after neutron irradiation. *Drug Dev Ind. Pharm*. 2008;34:796–806. doi:10.1080/03639040801918623

80. Smits MLJ, Nijsen JFW, van Den Bosch MAAJ, Lam MGEH, Vente MAD, Huijbregts JE. Holmium-166 radioembolization for the treatment of patients with liver metastases: design of the phase I HEPAR trial. *J Exp Clin Cancer Res*. 2010;29:70. doi:10.1186/1756-9966-29-17

81. Vente MAD, de Witt TC, van Den Bosch MAAJ, et al. Holmium-166 poly(L-lactic acid) microsphere radioembolisation of the liver: technical aspects studied in a large animal model. *Eur Radiol*. 2010;20:862–869. doi:10.1007/s00330-009-1613-1

82. Nijsen JFW, Zonnenberg BA, Woittiez JR, et al. Holmium-166 poly (L-lactic acid) microspheres applicable for intra-arterial radionuclide therapy of hepatic malignancies: effects of preparation and neutron activation techniques. *Eur J Nucl Med*. 1999;26:699–704.

83. Fujinaga T, Lee HL. Acetylacetone as chelating reagent, extracting solvent, and electrolysis medium: polarographic determination of uranium(VI) and iron(III). *Talanta*. 1977;24(6):395–396.

84. Afghan BK, Dagnall RM, Thompson KC. Inorganic polarography in organic solvents-III analytical applications of metal-acetylacetonate complexes in toluene. *Talanta*. 1967;14(7):715–720.

85. Steinbach JF, Freiser H. Acetylacetone as analytical extraction agent. *Anal Chem*. 1954;26(2):375–379.

86. Ganjali MR, Daftari A, Mizani F, SalavatiI-Niasarj M. Titanium acetylacetonate as an excellent Ion-carrier. *Bull Korean Chem Soc*. 2003;24(1):23–26.

87. Avinc O, Khoddami A. Overview of Poly(Lactic acid) (PLA) fibre. Part I: production, properties, performance, environmental impact, and end-use applications of Poly(lactic acid) fibers. *Fibre Chem*. 2009;41(6):391–401.

88. Hu YS, Zhang ZP, Song D, Bai DR, Wang YM. Preparation and properties of high strength rods from L- and D,L-lactide copolymer. *Chin J Polym Sci*. 2001;19(4):351–357.

89. Matsusaki H, Abe H, Doi Y. Biosynthesis and properties of poly(3-hydroxybutyrate-co-3-hydroxyalkanoates) by recombinant strains of *Pseudomonas* sp.61-3. *Biomacromolecules*. 2000;1(1):17–22.

90. Lee Y, Kim MK, Kim GJ, Chang HN, Park YH. Production of poly (β-hydroxybutyrate-co-β-hydroxyvalerate) from glucose and valerate in alcaligenes eutrophus. *Biotechnol.Lett*. 1995;17(6):571–574.

91. Holmes PA. Applications of PHB – a microbially produced biodegradable thermoplastic. *Phys Technol*. 1985;16(1):32–36.

92. Quental AC, de Carvalho FP, Tada ES, Felisberti MI. Blendas de PHB e seus copolímeros: miscibilidade e compatibilidade. *Quim Nova*. 2010;33(2):438–446.

93. Bult W, Seevinck PR, Krijger GC, et al. Microspheres with ultra-high holmium content for radioablation of malignancies. *Pharmaceut Res*. 2009;26(6):1371–1378.

94. Bitar R, Leung G, Perng R, et al. What every radiologist wants to know but is afraid to ask. *RadioGraphics*. 2006;26:513–537. doi:10.1148/rg.e24

95. Mazzola AA. Ressonância magnética: princípios de formação da imagem e aplicações em imagem funcional. *Revista Brasileira De Física Médica*. 2009;3:117–129.

96. Tilloy S, Bertoux F, Mortreux A, Monflier E. Chemically modified β-cyclodextrins in biphasic catalysis: a fruitful contribution of the host-guest chemistry to the transition-metal catalyzed reactions. *Catal Today*. 1999;48:245–253.

97. Mueller RH, Wallis KH. Surface modification of i.v. injectable biodegradable nanoparticles with poloxamer polymers and poloxamine 908. *Int J Pharm*. 1993;89:25–31.

98. Frank MM, Fries LF. The role of complement in inflammation and phagocytosis. *Immunol Today*. 1991;12(9):322–326. doi:10.1016/0167-5699(91)90009-I

99. Owens DE, Peppas NA. Opsonization, biodistribution, and pharmacokinetics of polymeric nanoparticles. *Int J Pharm*. 2006;307(1):93–102. doi:10.1016/j.ijpharm.2005.10.010

100. De Azevedo MBM, Tasic L, Fattori J, et al. New formulation of an old drug in hypertension treatment: the sustained release of captopril from cyclodextrin nanoparticles. *Int J Nanomedicine*. 2011;6:1005–1016.

101. Tanaka T, Azevedo MBM, Tanaka T, et al. Colorectal cancer chemoprevention by 2 -cyclodextrin inclusion compounds of auraptene and 4-geranyloxyferulic acid. *Int J Cancer*. 2010;126:830–840. doi:10.1002/ijc.24833

102. Bünzli JC, Piguet C. Taking advantage of luminescent lanthanide ions. *Chem Soc Rev*. 2005;34:1048–1077.

103. Diaz-Acosta I, Baker J, Cordes W, Pulay P. Calculated and experimental geometries and infrared spectra of metal tris-acetylacetonates: vibrational spectroscopy as a probe of molecular structure for ionic complexes. Part I. *J Phys Chem A*. 2001;105:238–244.

104. Colthulp NB, Day LH, Wiberley SE. *Introduction to Infrared and Raman Spectroscopy*. 3ª ed. London: Academic Press; 1990.

105. Oliveira LM, Araujo ES, Guedes SML. Gamma irradiation effects on poly(hydroxybutyrate). *Polym Degrad Stabil*. 2006;91:2157–2162.

106. Hussein GAM, Ismail HM. Characterization of lanthanium oxide formed as a final decomposition product of lanthanium acetylacetonate: thermoanalytical, spectroscopic and microscopic studies. *Powder Technol*. 1995;84:185–190.

107. Hussein GAM. Rare earth metal oxides: formation, characterization and catalytic activity. Thermoanalytical and applied pyrolysis review. *J Anal Appl Pyrol*. 1996;37:111–149.

108. Gonçalvez SP, Martins-Franchetti SM. Action of soil microorganisms on PCL and PHBV blend and films. *J Polym Environ*. 2010;18:714–719.

109. Kooijman H, Nijsen F, Spek AL, Schip FV. Diaquatris(pentane-2,4-dionato-O, O') holmium (III) monohydrate and diaquatris(pentane-2,4-dionato-O,O') holmium (III) 4-hydroxypentan-2-one solvate dehydrate. *Acta Crystallogr C*. 2000;56:156–158. doi:10.1107/s0108270199013566

110. Lakouraj MM, Tajbakhsh M, Mokhtary M. Synthesis and swelling characterization of cross-linked PVP/PVA hydrogels. *Iran Polym J*. 2005;14:1022–1030.

111. Song HT, Choi JS, Huh YM. Surface modulation of magnetic nanocrystals in the development of highly efficient magnetic resonance probes for intracellular labeling. *J Am Chem Soc*. 2005;127:9992–9993. doi:10.1021/ja051833y

112. Qin J, Laurent S, Jo YS, et al. A high-performance magnetic resonance imaging T2 contrast agent. *Adv Mater*. 2007;19(14):1874–1878.

113. Estelrich J, Sánchez-Martín MJ, Busquets MA. Nanoparticles in magnetic resonance imaging: from simple to dual contrast agents. *Int J Nanomedicine*. 2015;10:1727–1741. doi:10.2147/IJN.S76501

114. Li Y, Chen T, Tan W, Talham DR. Size-dependent MRI relaxivity and dual imaging with Eu0.2Gd0.8PO4·H2O nanoparticles. *Langmuir*. 2014;30(20):5873–5879. doi:10.1021/la500602x